Vol. 1 October, 1954 No. 3

MINERALOGICAL JOURNAL

CONTENTS

On the Thermal Transformation of Kaolinite and Halloysite ..... M. Nakahira...129

Biotite Crystals from the Myōgō-hō, Miyagi Prefecture, Japan ..... H. Minato, Y. Takano and T. Ichimura...140

Uranium Contents of Zircons in Granite ..... I. Hayase...147

The Crystal Structure of Orpiment (As_2S_3) Refined..... ..... N. Morimoto...160

The Number of Counts of Beta-rays Detected by an End-window Geiger-Mueller Counter .....N. Katayama...170

Short Communications

Parallel Intergrowth of Pyroxene and Amphibole in Plutonic Rocks..... T. Sueno...185

The Mineralogical Society of Japan

Department of Geology and Mineralogy, Faculty of Science, Hokkaido University, Sapporo, Japan

MINERALOGICAL JOURNAL

published by

The Mineralogical Society of Japan

EDITORIAL BOARD

Zyunpei HARADA, *Hokkaido University;* Teiichi ITO, *University of Tokyo;* (Chief) Nobuo KATAYAMA, *University of Tokyo;* Keiichi OMORI, *Tohoku University;* Ryôiti KIRIYAMA, *University of Osaka;* Seitaro TSUBOI, *University of Tokyo;* Takeo WATANABE, *University of Tokyo;* Toyofumi YOSHIMURA, *Kyushu University.*

Instructions to Contributors

Manuscripts of articles should be submitted to the executive editor, Nobuo Katayama, at the College of General Education, University of Tokyo, Komaba, Meguro-ku, Tokyo. The manuscript should be type-written with double space lines, and not exceed 20 sheets of normal type-writing paper. References of literature should be in accordance with the forms used in the pages of this journal.

Plates and figures should be capable of reduction to not more than 10 by 15 centimetres. Line drawings should be in black India ink on white drawing board, tracing paper, or coordinate paper printed in blue. Photographs should be positive glossy prints.

Two referees chosen by the Editorial Board read the manuscript of article submitted before it is accepted for publication.

Thirty reprints without cover will be furnished to the author free of cost and without previous notice from him. Additional reprints will be furnished at cost when ordered.

The price of the journal to subscribers in Japan is 200 yen for a single copy (not including postage), and to subscribers in other countries $ 1.00 (including postage).

Printed in Japan

MINERALOGICAL JOURNAL, VOL. 1, NO. 3, PP. 129-139, OCT., 1954

ON THE THERMAL TRANSFORMATION OF KAOLINITE AND HALLOYSITE*

MITSUOKI NAKAHIRA

Scientific Research Institute, Tokyo

ABSTRACT

The thermal dehydration behaviours and x-ray diffraction features of heated kaolinite and halloysite have been investigated, especially for the so-called meta-kaolin state.

The results on the thermal dehydration studies show that the dehydroxylization of well-crystallized kaolinite is likely to take place with two steps, the first of which starts at about 520°C. Approximately one fourth of hydroxyl groups are expelled gradually between 650°C and 950°C. This is the second step of dehydroxylization. A crystalline-like structure is proposed for the first step of dehydroxylization.

It is also pointed out that the hydroxyl groups of halloysite are easily expelled, but the recombination of the destroyed structure to a new phase needs much more energy than in the case of kaolinite.

Introduction

Numerous studies on the thermal transformation of kaolinite and halloysite have, hitherto, been in good agreement in regard to a characteristic sequence of transformation. At approximately 500°C the liberation of hydroxyl groups starts, and at a temperature somewhat lower than 1000°C the mullite crystallization begins. Between these temperatures the so-called "meta-kaolin" state exists, and it is in this state that the details regarding the structural change are obscure. As the X-ray diffraction lines of this meta-kaolin state are very poor and diffuse, it is rather difficult to interprete these diffraction effects from the structural standpoint. For the purpose of

* The summary was read at the 3rd International Congress of Crystallography in Paris, July, 1954.

this study, besides the thermal and X-ray methods, the measurement of dielectric properties of this state would be a powerful means, and it is also of importance to trace the variations of X-ray diffraction patterns of the same specimens before and after the prolonged heating. In the course of my studies, the comparisons between these variations and the thermal dehydration behaviours made it possible to get some informations concerning the structural change at the meta-kaolin state, so that the present paper mainly dealt with these thermal dehydration and X-ray studies on this meta-kaolin state.

Specimens used were the Kanpaku* kaolin and the Ina** clay; the former is a well-crystallized kaolinite and the latter is a typically two-dimensional hydrated halloysite. The former contains a small amount of quartz as impurity which remains inert to 1,100°C, while the latter is nearly pure. Details on these clays have been described by K. Ôshima *et al.*[5)6)] and the author[4)].

Experimental procedures

Thermal dehydration studies on these two specimens were carried out with a heating rate of about 2°C per minute, using a thermobalance of usual type reconstructed from a chemical balance. The sensitivity of this balance is 0.1 milligram. About 300–400 milligrams of specimens were used.

Generally speaking, it can be pointed out that the dehydration curve itself does not represent the equilibrium state at each temperature, so that, some of the equilibrium experiments were also carried out; specimens were heated to various temperatures with the same rate of heating as above mentioned and left at each temperature until there could not be observed any more weight loss. Results, thus obtained, are summarized in Figs. 1~3.

---

* Kanpaku-Mine, Kawachi-Gun, Tochigi Prefecture, Japan. (栃木県河内郡関白鉱山)

** Ina-machi, Kami-Ina-Gun, Nagano Prefecture, Japan. (長野県上伊那郡伊那町)

X-ray works were carried out using Norelco spectrometer. Specimens were heated to various temperatures with the same rate of heating as used in dehydration experiments and left at these temperatures for three hours and air quenched to be subjected to X-ray analysis. Supplementary specimens were heated to comparable temperatures with the same rate of heating as mentioned above, and withdrawn without soaking to trace the variations of diffraction patterns before and after the prolonged heating.

Thermal dehydration and equilibrium curves

Kanpaku kaolin (a well-crystallized kaolinite): The dehydration curve (Fig. 1 (a)) shows that the dehydroxylization starts at about 520°C and approximately three fourth of hydroxyl groups are expelled between 520° and 650°C, and the liberation of the remainder seems to occur gradually up to 950°C. This tendency of dehydration process can be seen in many experimental curves in various

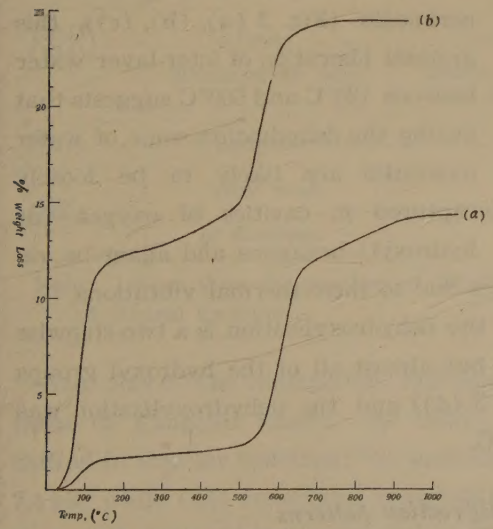

Fig. 1. Dehydration curves.
(a) Kanpaku kaolin (a kaolinite)
(b) Ina clay (a hydrated halloysite)

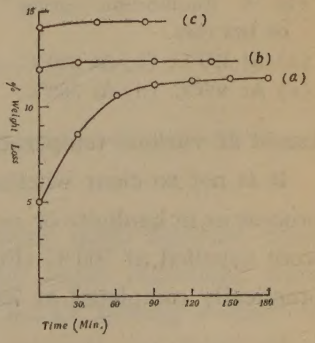

Fig. 2. Equilibrium curves of kanpaku kaolin.
(a) At 570°C, (b) At 700°C, (c) At 950°C.

literatures, but no explanation has so far been tried out.

Equilibrium experiments (Fig. 2) show such a tendency much more clearly. At 570°C (Fig. 2 (a)), approximately three fourth of hydroxyl groups were actually expelled, but the liberation of the remainder did not take place at this stage. Even at 700°C (Fig. 2 (b)) a small amount of hydroxyl groups persisted, and at 950°C (Fig. 2 (c)) the dehydroxylization was finally completed.

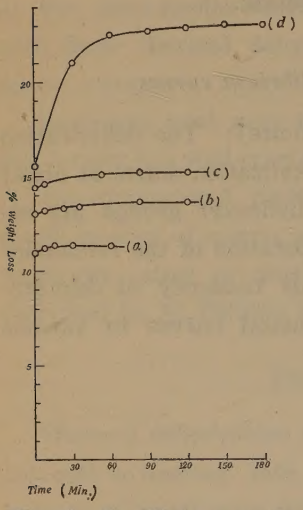

Fig. 3. Equilibrium curves of Ina clay.
(a) At 120°C, (b) At 240°C, (c) At 400°C, (d) At 500°C.

Ina clay (a hydrated halloysite): The dehydration curve (Fig. 1 (b)) shows that approximately 80~90% of adsorbed and inter-layer water were easily expelled between 50°C and 120°C, but the remainder of inter-layer water were released gradually up to 500°C, where the liberation of hydroxyl groups began. Furthermore, as can be seen in the equilibrium experiments (Fig. 3 (a), (b), (c)), this gradual liberation of inter-layer water between 120°C and 500°C suggests that during the dehydration some of water molecules are likely to be loosely captured in cavities of oxygen (or hydroxyl) hexagons and again be released at various temperatures due to their thermal vibrations.

It is not so clear whether the dehydroxylization is a two-stepwise process as in kaolinite or not, but almost all of the hydroxyl groups were expelled at 500°C (Fig. 3 (d)) and the dehydroxylization was practically completed at 700°C.

X-ray diffraction patterns

Kanpaku kaolin: At 570°C the basal and (060) reflections easily disappeared, the (200) reflection was very diffuse and weakened, and

the others except the (020) reflection were almost extinguished; while the (020) reflection always persisted clearly at about its original position. At 700°C the (020) reflection, though rather two-dimensional, still persisted at about its original position, while the (200) reflection was further weakened. At 950°C the (020) reflection itself shifted slightly to the high angle side and changed into a diffuse peak corresponding to about 4.1 kX; furthermore, it was seemingly that two of the very diffuse lines of mullite were detected. These are summarized in Table 1. The formation of γ-alumina could not be detected with this specimen.

Table 1. Main features of X-ray diffraction patterns.

Original	at 570°C	at 700°C	at 950°C
(02 *l*), (11 *l*)	→ (020) with some amounts of tailed reflections	→ (020) tailed reflection	very diffuse band with its peak at about 4.1 kX
(20 *l*), (13 *l*)	→ (200) diffuse, weak band	→ (200) diffuse, very weak band	→ disappear
(00 *l*)	→ disappear		
(060)	→ very weak or disappear	→ disappear	

Note: Indices show the positions of diffraction peaks correlated with those of original kaolinite.

Ina clay: The diffraction features were quite different from those of Kanpaku kaolin. At 500°C, the basal reflections were shifted to smaller spacings; for instance, 10.1 kX spacing reduced to 7.4 kX, while (*hk*) reflections remained unchanged. At 600°C, all of these diffraction lines disappeared and only a very diffuse band with its peak near 4.0 kX was detected. At 950°C, some faint lines of γ-alumina were observed, while the band remained unchanged.

Discussions

From the thermal dehydration and equilibrium curves, compared with the X-ray diffraction features, the author considers that the liberation of hydroxyl groups of Kanpaku kaolin (a well-ordered kaolinite) is likely to take place with two steps and approximately one forth of hydroxyl groups may be expelled gradually between 650°C and 950°C, while the dehydroxylization of Ina clay (a random layer lattice mineral) can be completed much more easily than the Kanpaku kaolin. The X-ray diffraction features of Kanpaku kaolin at 570°C shows that the b-periodicity of oxygen frame-work is not disturbed and the a-periodicity is slightly random, while the c-periodicity is completely destroyed.

It may be supposed that, in a well-ordered kaolinite, the first step of liberation of hydroxyl groups might be a reaction between hydroxyl groups situated at the outmost side of kaolinite layer, and, in consequence, the net result would be such that the edge-shared zigzag chains of hydroxyl octahedrons in a kaolinite layer would change to face-shared chains parallel to the original a-axis with the remainder of hydroxyl groups, which are originally situated in the middle position of layer, being shared between neighbouring chains. Johns[3] has suggested that, by analogy with the anhydride of pyrophyllite type mineral proposed by Bradley and Grim[1], there must be face-shared zigzag chains of octahedral units in the meta-kaolin state. However, as illustrated in Fig. 4 (b), in order to produce such a chain it is necessary for the hydroxyl groups in the middle of layer to remain and be shared between neighbouring chains. Thus, the liberation of hydroxyl groups, which are situated at the outmost side of the layer, merely results in slight rotation of octahedral units in such directions as indicated by arrows in Fig. 4 (a), being followed by the formation of face-shared zigzag chains as illustrated in Fig. 4 (b). (The arrows indicate merely an example of rotation. There can be other sets of rotation which will result

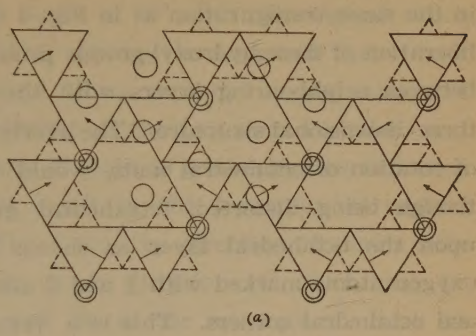

Fig. 4. Schematic representation of structural layer viewed perpendicular to it.
(a) Chains of octahedral units in the original layer.
Dotted line shows outmost side of layer (OH groups of this site are not shown in the figure. They occupy the corners of octahedrons.) Full line shows arrangement of O and OH in the middle of layer. (O atoms of this site are not shown in the figure. They also occupy the corners of octahedrons.)
◎ : OH groups in the middle of layer.
○ : O atoms overlying upon these octahedral chains. Only a part of these oxygen atoms are shown in the figure. Overlying Si atoms are not shown.

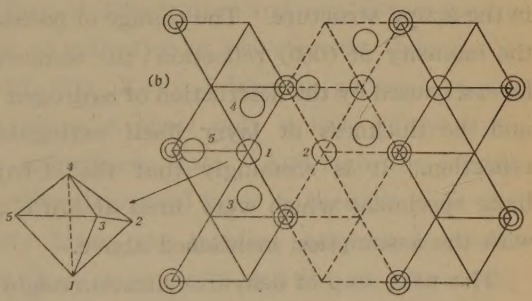

(b) Face-shared octahedral chains.
◎ } The same with those
○ } in (a).
Full and dotted lines show neighbouring chains. Numbers indicate oxygen atoms corresponding to face-shared Si-O tetrahedrons shown on the left side of the figure.

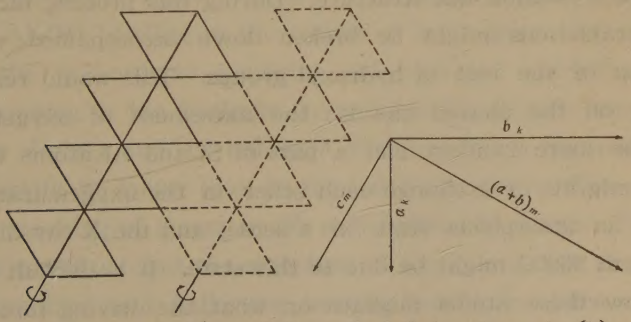

(c) Octahedral chains caused by splitting off of chains shown in (b). Full and dotted lines indicate neighbouring chains. Figure on the right side shows the mutual orientation of the axes of kaolinite and mullite.
Suffix k : kaolinite. m : mullite.

in the same configuration as in Fig. 4 (b).) At the same time, the liberation of these hydroxyl groups probably destroys the interaction between neighbouring layers with the result of disappearance of three-dimensional structure. The overlying silica layer, as the result of rotation of octahedral units, would change to many face-shared, though being distorted, tetrahedral groups seperately distributed upon the octahedral layer as shown in Fig. 4 (b). In Fig. 4 (b), oxygen atoms marked with 1 and 2 are shared between tetrahedral and octahedral corners. This is a very unstable form which will easily be rendered to its breakdown.

It should now be pointed out that the configuration shown in Fig. 4 (b) is an idealized one, and, therefore, the coordinates of each atom, especially z and x coordinates, might be somewhat random in the actual structure. The change of positions of Al atoms reduces the intensity of (060) reflection; the somewhat irregular stacking of layers, caused by the destruction of hydrogen bonding between layers, and the thickness of layer itself extinguish the (00 *l*) and (*hkl*) reflection. It is seemingly that the X-ray diffraction features of those specimens which were fired at 570°C and 700°C are in accord with the assumption mentioned above.

The next step of dehydroxylization might be a process of breaking down this crystalline-like structure. During this process, face-shared Si-O tetrahedrons might be broken down accompanied with the liberation of the rest of hydroxyl groups. This would result in a splitting off the shared chains; the movement of oxygen atoms would be more random and a part of Si and Al atoms would be able to migrate or exchange each other in the oxygen frame-work. This is an amorphous state in a sense, and the X-ray diffraction features at 950°C might be due to this state. It is difficult to make clear how these atoms migrate or what the driving force of this migration is, but the parallel chains of octahedral units in the first step of dehydroxylization have a favourable configuration of oxygen atoms to reproduce the edge-shared chains in such a direction that

the axis of chain makes an angle of 30° with the original a-axis parallel to the layer (Fig. 4 (c)). It may be supposed that a part of overlying oxygen atoms would fill up vacancies at the corners of octahedral units caused by splitting off the face-shared chains, and a slight rotation around the axis of chain in a direction as indicated by arrows in Fig. 4 (c) would result in the formation of mullite crystals. As illustrated in Fig. 4 (c), the direction of chains may be that of c-axis of mullite, the (a+b) direction of which may be perpendicular to this c-axis and lie in the same plane. Such an orientation of mullite crystal to its original kaolinite has been observed by Comeforo, Fischer and Bradley[2]. The periodicities thus produced are c=5.95 kX and a+b=10.3 kX, which are comparable to those of mullite.

On the contrary, the thermal dehydration and equilibrium curves of hydrated halloysite show no indication of two-stepwise dehydroxylization. In accordance with this, X-ray diffraction patterns at any temperatures of dehydroxylization show only a very diffuse band which is ascribed to an amorphous state. Although the atomic configuration in the halloysite structural layer is thought to be the same with that of kaolinite layer, the bonding between hydroxyl groups may be more loose than in kaolinite and the structure may be easily destroyed upon heating. The author considers that the nature of Al–OH bonding in the middle of layer differs slightly each other in the well-ordered kaolinite and hydrated halloysite. The stronger bonding in the kaolinite layer probably distorts the structural layer slightly and the influence of a layer upon its neighbouring layer might be larger than in the halloysite layer. This causes an unique stacking of layers in the well-ordered kaolinite. That is, the author considers that the structure of layer is nearly the same in both kaolinite and halloysite, but the details are different each other. Recently the author has examined a poorly organized kaolinite, the thermal behaviour of which has the resemblance of that of hydrated halloysite. (Details will be reported in the near future.)

While the destruction of structure in the hydrated halloysite is much more easy, recombination of this destroyed structure to a new phase, mullite or cristobalite, seems to need much more energy than in the case of kaolinite. It is noticable that the formation of poorly organized γ-alumina prior to the mullite-crystallization can be detected in the case of halloysite or disordered kaolinite, while in well-ordered kaolinite it does not seem to occur.

Conclusions

It is possible to suppose that the dehydroxylization of well-ordered kaolinite takes place in two-steps, the first of which does not necessarily result in a so-called amorphous state but a crystalline-like structure may be produced as in Fig. 4 (b); while the dehydroxylization of hydrated halloysite is much more easily performed and the two-stepwise character can not be detected in this case. These behaviours suggest that the nature of hydroxyl bondings in the structural layers of these two minerals are different each other; the unique structure of well-ordered kaolinite and the random structure of hydrated halloysite may be ascribed to this difference.

Though we can not obtain a sufficiently large crystal to try a Fourier analysis of (hk 0) reflections, the author considers that the thermal behaviours of kaolinite and halloysite indicate this structural difference.

Acknowledgements

The writer wishes to express his hearty thanks to Mr. K. Kuroda of the Tokyo Institute of Technology for his intimate assistance in the course of thermal dehydration experiments. Further acknowledgements are due to Mr. S. Iwai of the same Institute to whom the writer owed the specimens used in this study.

References

1) Bradley, W. F. and R. E. Grim: Amer. Miner., 36, 182, (1951).
2) Comeforo, J. E., R. B. Fischer and W. F. Bradley: J. Amer. Ceramic Soc., 31, 254, (1948).
3) Johns, W. D.: Min. Mag., 30, 186, (1953).
4) Nakahira, M., S. Iwai and A. Suzuki: J. Sci. Research Inst., 45, 52, (1951).
5) Oshima, K., H. Yamada and K. Hata: Ceramic Raw Materials. Vol. II, 170, (1949). (in Japanese)
6) Oshima, K. and Y. Ueno: Ceramic Raw Materials Vol. III, 1, (1949). (in Japanese)

Manuscript received August 18, 1954.

MINERALOGICAL JOURNAL, VOL. 1, NO. 3, PP. 140-146, OCT., 1954

BIOTITE CRYSTALS FROM THE MYŌGŌ-HŌ, MIYAGI PREFECTURE, JAPAN*

HIDEO MINATO and YUKIO TAKANO

Institute of Earth Science, College of General Education, University of Tokyo

TAKESHI ICHIMURA

Institute of Earth Science, Faculty of Education, Yamagata University

ABSTRACT

The biotite crystals described in this paper are found as an ingredient mineral of hornblende biotite granite exposed on Myōgō-hō, Kawasaki-machi, Shibata-gun, Miyagi Prefecture. They are also contained abundantly in the sand derived from the weathered rock. These crystals occur as six-sided short prisms or plates. Hardness: 2.5~3. Colour: brownish black with brownish streak. Indices of refraction: $\alpha = 1.620 \sim 1.621$, $\beta = 1.658$, $\gamma = 1.658 \sim 1.659$. Further, they are characterized by the small optic angle [$(-)2V \fallingdotseq 0°$] and weak dispersion ($v > \rho$). A chemical analysis gave the following result for this mineral: SiO_2 33.92, TiO_2 2.91, Al_2O_3 13.88, Fe_2O_3 3.39, FeO 26.66, MnO 1.35, MgO 4.86, CaO 0.75, K_2O 7.46, Na_2O 1.70, H_2O (+) 3.53, H_2O (−) 0.16, total 100.57%. Moreover, the X-ray powder diagram of this specimen agrees with that of biotite rich in ferrous iron on its octahedral layer.

Introduction

In the summer of 1950, some biotite crystals were obtained by one of the writers (H. M.) from Myōgō-hō, Kawasaki-machi, Miyagi Prefecture** (Fig. 1). Some specimens from this locality do not expand by heating and appear fresh under the microscope. They have

* Dedicated to Dr. S. Tsuboi, Emeritus Professor of the University of Tokyo on the occasion of his sixtieth birthday.

** 宮城県柴田郡川崎町名号峰.

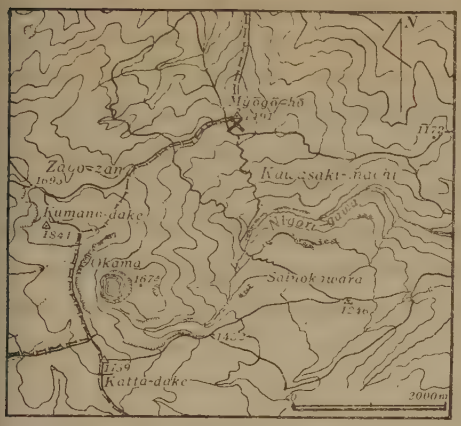

Fig. 1. Map showing the locality of biotite (×).

been investigated by the optical and chemical as well as by the X-ray powder method.

This paper is dedicated to Emeritus Professor Seitaro Tsuboi who has carried out interesting investigations on the biotite in the granitic rocks in Japan.[5]

Occurrence

Myōgō-hō, the locality of this biotite crystal, is situated in the outer zone of the northeastern part of the Zaō volcanic area and is accessible from the Shiroishi or Oogawara station of the Tōhoku Railway Line *via* the Gaga hot spring. It is built up, at the western part of the area, of hornblende biotite granite which is covered by the olivine-bearing two-pyroxene andesite and its ejecta erupted from the Zaō volcano.[3] Biotite crystals are found on the summit where the granite is disintegrated into sands and gravels. They are found together with feldspar and hornblende which are also component minerals of the granite.

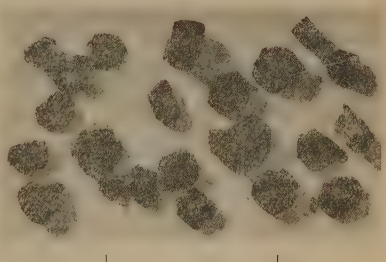

2 cm

Fig. 2. Photograph of the biotite crystals from Myōgō-hō.

Petrography of hornblende biotite granite

It shows a granular texture, with a porphyritic appearance due to the presence of large microcline crystals (2×0.7×0.7 cm). Main

component minerals are biotite, orthoclase, with sporadic microcline structure, plagioclase and granular quartz; and they are associated by a small amount of hornblende and minute crystals of iron oxide mineral, zircon, allanite, etc.. The chemical analysis (by Minato in 1954) follows, SiO_2 69.48, TiO_2 0.61, Al_2O_3 15.35, Fe_2O_3 1.97, FeO 2.68, MnO 0.39, MgO 0.77, CaO 3.09, K_2O 2.99, Na_2O 1.54, P_2O_5 0.22, H_2O (+) 1.03, H_2O (−) 0.29, total 100.41%. Hence, the mother rock is rather rich in iron and calcium but poor in alkalies as compared with normal granites; this may be due to the abundance of biotite and plagioclase.

General characters

The biotite crystals from Myōgō-hō, brownish black in colour, have a six-sided short prismatic or platy form, occurring frequently together with quartz and feldspar which are attached to the surface of the samples and also found as inclusions. In addition, there are minor inclusions of magnetite and zircon. Observed forms are *c*(001), *b*(010) and *m*(110), with a perfect cleavage parallel to (001) and a parting parallel to (010). The hardness is 2.5~3. Their cleavage flakes have a brownish gray colour and are very flexible.

Optical properties

Seven crystals were optically investigated. Of these, six crystals used for chemical analysis gave the following indices of refraction:

α=1.620, β=1.658, γ=1.658, $\gamma-\alpha$=0.038 and (−)2V nearly 0°.

The refractive indices β and γ were measured on six crystals and α was determined on two of the large crystals, and all of them gave the same results. The similar indices of refraction are also shown by the other remaining crystal, viz.,

α=1.621, β=1.658, γ=1.659.

Dispersion ($v > \rho$) is weak. They are strongly pleochroic, viz., X=

pale brown or yellow, Y=dark brown, Z=dark brown. X is nearly normal to (001).

Chemical composition

Material for chemical analysis was obtained by a hand sorting method from the thin cleavage flakes under the binocular microscope. Before the chemical analysis was carried out, they were examined under the petrographic microscope with high-power objective. The examination showed that the material contained no appreciable amount of impurity. Moreover, six crystals, as mentioned above, have the same optical properties. They were chemically analysed by means of semi-micro methods. The results are given in Table 1, and the atomic ratio was calculated from the weight

Table 1. Chemical analysis and atomic composition of the biotite crystal from Myōgō-hō.

	Wt. %	Mol. prop.	Atom. ratio	
SiO_2	33.92%	.565	Si 2.76	4.00
TiO_2	2.91	.036	Al 1.24	
Al_2O_3	13.88	.135		
Fe_2O_3	3.39	.021	Al 0.08	
FeO	26.66	.371	Ti 0.18	
MnO	1.35	.019	Fe^{+3} 0.21	2.96
MgO	4.86	.121	Fe^{+2} 1.81	
CaO	0.75	.013	Mn 0.09	
K_2O	7.46	.079	Mg 0.59	
Na_2O	1.70	.027	Ca 0.06	
H_2O (+)	3.53	.196	K 0.77	1.09
H_2O (−)	0.16	.010	Na 0.26	
Total	100.57			

Analysed by H. Minato. (1954)

percentage. Chemical formula is given as $(Ca_{0.06}\ Na_{0.26}\ K_{0.77})\ (Ti_{0.18}\ Mn_{0.09}\ Mg_{0.59}\ Fe^{+2}{}_{1.81}\ Fe^{+3}{}_{0.21}\ Al_{0.08})\ (Al_{1.24}\ Si_{2.76})\ O_{10}\ (OH)_{2.00}$. It shows fair agreement with the chemical analysis of some

biotite crystals contained in granitic rocks from Nada-mura, Yamaguchi Prefecture and Sanage-yama, Aichi Prefecture, as reported by Tsuboi, Sugi and Iwao.[5]

X-ray investigation

Carefully hand-sorted material of this biotite was used for the experiment of X-ray powder method by means of Philips "Norelco" X-ray spectrometer. The observed intensities and measured spacings are listed in Table 2 together with those by Nagelschmidt[4] for comparison. The values are also compared with the indices and calculated values, and a close agreement was found between them. The facts that the spacing of (060) is observed in 1.529 Å and not in 1.50 Å, and the intensity of (002) reflection appears weak, suggest the specimen to be a trioctahedral mica such as biotite[2,6]. Furthermore, that the intensity of (003) reflection is stronger than that of (005) is one of the characteristics of the high ferriferic type of octahedral layer in mica mineral[2]. According to the consideration on the order of the intensities (Cu Kα) observed on (00l) reflections, such as (001), (003), (005), (002) and (004), the biotite specimen of this locality has the ratio of Mg/Fe between 1/2 and 1/5 in the octahedral layer. The result agrees fairly well to the value of 1/3 obtained by the chemical analysis. The correlation between the intensity of (00l) reflection and the ratio of Mg/Fe has been attempted by Grim, Bradley and Brown.[1]

Acknowledgements

The writers wish to offer their sincere thanks to Professor Teiichi Ito of the Institute of Mineralogy, University of Tokyo, for his kind help during the present work, especially in the X-ray investigation. Further acknowledgements are due to Mr. Mitsuoki Nakahira of the Scientific Research Institute for his useful suggestions in the X-ray experiments.

Table 2. X-ray powder data of biotite.

Myōgō-hō				after Nagelschmidt[4]		Calculated value	
I(CuKα)*	d	I(FeKα)**	Q obs.	I(FeKα)**	Q obs.	Q calc.	(*hkl*)
18	14.17 Å	55	0.0047				
25	11.81	63	0.0081				
100	10.16	100	0.0096	vs	0.0098	0.0098	(001)
26	5.01	24	0.0386			0.0392	(002)
		24	0.0464	w	0.0477	0.0480	(110)
		26	0.0642				
24	3.72	42	0.0729				
		31	0.0797				
100	3.75	31	0.0884	vs	0.0886	0.0880	(003)
23	3.20	28	0.0989	vw	0.1008		
21	2.95	26	0.1166	vw	0.1181	0.1144	(103)
22	2.65	38	0.1426	s	0.1424	0.1448	(200)
37	2.519	37	0.1576	w	0.1587	0.1564	(004)
21	2.447	34	0.1654	s	0.1666	0.1664	(211)
		26	0.1924	vv	0.1920	0.1920	(220)
		(28	0.2024				
20	2.184	(30	0.2079	s	0.2099		
29	2.013	36	0.2463	s	0.2495	0.2450	(005)
18	1.920	24	0.2548	vw	0.2738		
18	1.830	26	0.2912				
		23B	0.3146	vw	0.3257		
23	1.677	(27	0.3452				
		(37	0.3551	s	0.3577	0.3528	(006)
20	1.550	37	0.4083		0.4156		
20	1.529	26	0.4283	s	0.4288	0.4248	(060)
		24	0.4535	vw	0.4577		
20	1.438	28	0.4824	vw	0.4904		
17	1.418						
17	1.409	24	0.5074				
		26	0.5252				
		30	0.5337	w	0.5399		
17	1.314	27	0.5741	w	0.5618		
17	1 304	25	0.5862	w	0.5827		
17	1.258	26	0.6309				
		(24	0.7418				
		(24	0.7457				
		23B	0.7599				
		24B	0.7722				
		23B	0.7764				
		23B	0.7776				
		23	0.7930				
		23	0.7974				

B: Broadly spreading band

*) "Norelco" X-ray spectrometer CuKα1, λ=1.54050 Å. No filter. slit 1°, 0.006", 1°. Scanning speed 2°/min. Scalefactor 4. Multiplier 1. Time constant 4 sec.

**) "Norelco" X-ray spectrometer FeKα1, λ=1.93597 Å. No filter. slit 4°, 0.006", 4°. Scanning speed etc. are the same as above.

REFERENCES

1) Bradley, G. W.: X-ray Identification and Crystal Structures of Clay Minerals (London), 163 (1951).
2) Grim, R. E.: Clay Mineralogy (New York), 93 (1953).
3) Ichimura, T.: Bull. Earthq. Res. Inst., **29**, 327 (1951).
4) Nagelschmidt, G.: Zeit. Krist., **97**, 514 (1937).
5) Tsuboi, S., K. Sugi and S. Iwao: Jour. Geol. Soc. Jap., **45**, 453 (1938). (in Japanese)
6) Walker, G. F.: Miner. Mag., **28**, 73 (1953).

Manuscript received August 3, 1954.

Mineralogical Journal, Vol. 1, No. 3, pp. 147-159, Oct., 1954

URANIUM CONTENTS OF ZIRCONS IN GRANITE*

Ichikazu Hayase

Geological and Mineralogical Institute, Faculty of Science, University of Kyoto

Abstract

Zircon grains, isolated from the granite exposed at Kitashirakawa in the suburbs of Kyoto City, are separated under the binocular microscope into two main groups: the transparent grains and the cloudy ones covered with micro-fissures. Each zircon grain is fused into a NaF bead. The examination of the bead by fluorescent method reveals that the transparent group is much lower in uranium content than the other. The uranium behavior in the zircon grain is treated both petrologically and geologically.

Introduction

Among many reports bearing on the title above given, that by Hutton[4] treats the rare elements contained in heavy minerals, among which I am especially interested in zircon and in its divergent order of radioactivity as I have already pointed out elsewhere.[2]

Almost perfect zircon crystals are easily obtained from weathered granite by panning, magnetic and heavy liquid separation, because they have undergone less weathering than quartz, feldspar and biotite. Such a zircon crystal is at first examined under the binocular microscope, then fused on the gas burner into a NaF bead, and finally exposed to ultra-violet light to reveal its uranium content. Though the two results from the autoradiographic and fluorescent experiments well agree with each other, it is to be noticed that by the fluorescent method a) in each minute grain its size, crystal, colour and so on are well discernible under the binocular microscope and

* Read at the meeting of Kansai Branch of the Geological Society of Japan on October 24, 1953.

b) what can be measured is the uranium content alone, whereas by the autoradiographic method it is merely the sum total of all radioactive elements contained in the grain.

Quantitative fluorescent method

In my experiment I used a platinum wire of 0.5 mm in diameter, about 3 mm in diameter of its loop, and a quartz mercury lamp (100 V, 1.5 A. D.C.) equipped with a UV DI (Tokyo-Shibaura Co. Ltd.) glass-filter as the ultra-violet light source. The uranium content was measured by comparing the effect of each experiment with that of standard beads of a certain uranium content.[6] It must be remembered that not the size of the bead, but the density of the uranium fused into it, determines the order of the fluorescence.

If the standard bead A (containing U_a gram of uranium per gram of NaF) and the bead B (containing U_b gram of uranium per gram of NaF) give, in experiment, the same order of fluorescent light, then $U_a = U_b$ ..... (1)
Denoting the weight of NaF in the bead B by B, the uranium content in the bead B is equal to $U_a \times B$. (In this experiment all the beads weighted about 30 mg.)

Because of its simple tetragonal form, the volume of a zircon crystal can be determined under the binocular microscope and, the specific gravity of zircon being 4.7, the weight of the crystal (Z gr.) is also measurable. A minute zircon crystal (some 0.1 mm in length), placed upon a glass slide, can be fastened to a heated NaF bead, whose blankness of uranium has already been tested. For precise measurement of the weight of a NaF bead, it is better to make the platinum wire, which is to be measured together, removable from its glass holder. As is obvious from formula (1), the uranium content of the zircon grain is $U_b \times B \times 100/Z$ per cent. In comparison with the NaF of the bead, the zircon grain treated here is negligibly small in weight (about 0.01 mg). Therefore, though open to the

question of interferent elements, such as rare earths, beryllium and so on,[6][7] the fluorescent method is, nevertheless, applicable to the quantitative measurement of uranium content, for, however abundant those elements may be in zircon, the weight of the whole grain itself is but negligible.

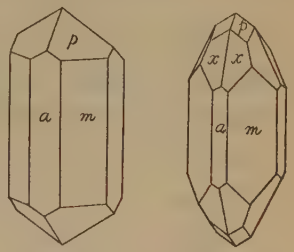

(A) (B)

Fig. 1. Habit of Kitashirakawa zircons. *a*(100), *m*(110), *p*(111), *x*(311).

Habit of Kitashirakawa zircons

The zircon grains obtained even from the same granite sample are manifold in grain size, colour and microfissures. In their crystallographic features most grains belong to the normal form as shown in Fig. 1(A), which is mainly made of a pyramid *p* and prisms *a* and *m*, sometimes with very narrow *x*. In rare cases there are zircons, as shown in Fig. 1(B), whose crystal faces *a*, *x*, *p* and *m* are so developed that they look like round grains.

As a rule, long prismatic zircon grains belong to the transparent group and are less brittle than the cloudy group covered with microfissures. Generally speaking, many zircon crystals, containing much inclusion, have a cloudy core.

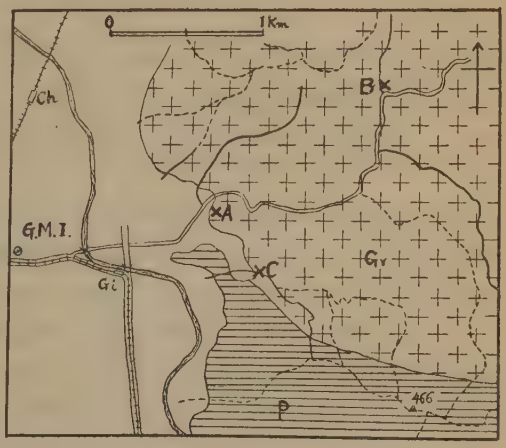

Fig. 2. Geological map of Kitashirakawa.
G. M. I.: Geological and Mineralogical Institute, University of Kyoto.
Ch.: Chayama Station.
Gi. : Ginkakuji-michi.
Gr. : Kitashirakawa Granite.
P. : Palaeozoic formation.

Transparent zircons

As for the transparent crystals obtained from locality A (see Fig. 2), it was found that the majority of zircons containing less than 0.09 per cent uranium belonged to the colourless, and those of the pink kind were rare. As shown in Fig. 3, the majority of forty two transparent grains were between 0.02 and 0.03 per cent in uranium content. As this order of uranium content is not uncommon among zircons, it is supposed to have been primordial. In zircons of this sort no fixed relation is found between the grain size and the radioactivity.

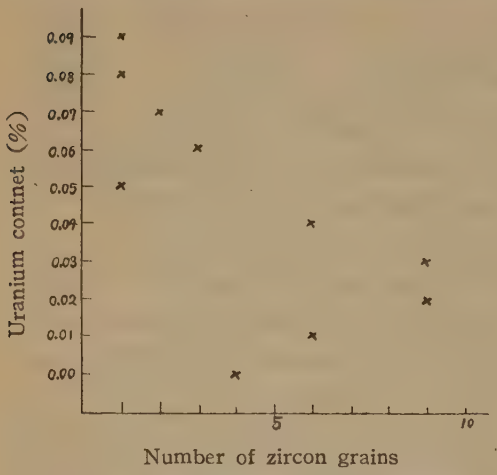

Fig. 3. Uranium contents of the transparent zircons from locality A (Fig. 2).

This sample was gathered from grains smaller than 62 mesh (containing biotite, albitic plagioclase, rarely orthoclase and quartz), sieved out of the weathered, not artificially crushed, granite.

Nine crystals obtained from the stream sand (locality B) showed the same order of uranium contents (see Fig. 4). Thirteen transparent grains from locality C revealed a quite different tendency (see Fig. 5), in which the range of uranium content was much wider than the others due to that locality C lies close to the margin of the Kitashirakawa granite mass where, as already ascertained by the autoradiographic method, the uranium content of zircon generally stands much higher than in the center of the mass, as at localities A and B.

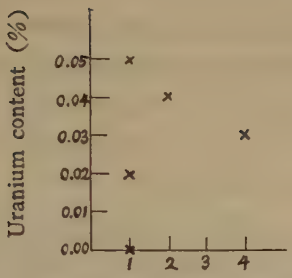

Fig. 4. Uranium contents of the transparent zircons from locality B (Fig. 2).

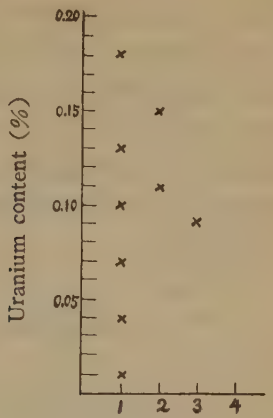

Fig. 5. Uranium contents of the transparent zircons from locality C (Fig. 2).

Zircons with microfissures

This group of zircons found at locality A was high in uranium content, as shown in Fig. 6, containing most frequently 0.2 per cent uranium, though its range was very wide (0.1~0.7 per cent.) It is to be noticed, however, that the transparent grains, though seldom, also amount to this order of uranium content. Microfissures occur in zircons due to uranium and process of rock weathering. Therefore, zircons included in a persistent host mineral like quartz remains transparent, though rich in uranium. The causes of such a diversity in uranium content among zircon grains belonging to

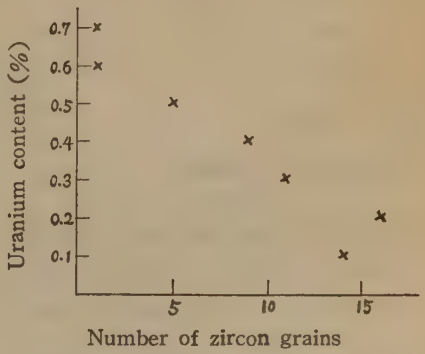

Fig. 6. Uranium contents of the zircons with microfissures from locality A (Fig. 2).

this group remains unsettled at present, but the result obtained from fifty samples showed that, grains containing 0.5 per cent uranium are about $(80\,\mu)^2$, whereas those with about 0.1~0.2 per cent uranium are some $(120\,\mu)^2$, in their basal section. In finer grains their large surface efficiency seems, in comparison with their volume, to have had relationship with their rich uranium content, as will be explained later.

Transparent coloured zircons

Zircons slightly coloured pink or yellow, under the binocular microscope, showed no great difference in size and shape from the other two groups. This group was generally found to be higher than the colourless ones in uranium content, though quite divergent (Table 1).

Table 1. Zircons taken out of fresh quartz and feldspar.

Colour of zircon	Uranium content (%)
Transparent	0.18 0.17 0.13
Brown	0.26
Pink	0.12
Yellow	0.11
Pale yellow-pink	0.10
Pale yellow	0.31 0.25 0.21(2*) 0.16 0.15 0.14 0.12 0.04 0.004 0.003
Pale pink	0.07 0.04 0.03(2) 0.02(3)

* Number of samples

Coloured zircons are rare in number, but divergent both in colour and in uranium content. In general the pale yellowish zircons are higher in uranium content than the pale pink ones.

Zircon with uneven distribution of uranium

The zircon grains treated hitherto contained uranium of uniform distribution, as can be ascertained from the fact that, when the

grain is divided into two, each of the two pieces gives nearly the same order of fluorescence.

Interesting, though rarely seen, are the grains which are, not all over, but partly covered with microfissures; for example, there are some acicular crystals, one end of which is cloudy with microfissures. It is highly probable that, during the panning procedure, its cloudy part falls away from the original crystal, owing to its greater brittleness than its transparent part. Such a grain can easily be broken, under the microscope, into two pieces just at the joint of the cloudy and the transparent parts, and when the two parts were tested separately by the fluorescent method, the cloudy part with microfissures was found to be much higher in uranium content than the transparent, as had already been expected from autoradiographic studies[1)2)]. Table 2 shows the result of the six grains obtained

Table 2. Heterogeneous zircon.

Sample	Uranium content of transparent part	Uranium content of turbid part
1	0.040%	0.084%
2	less than 0.002	0.062
3	0.008	0.019
4	0.081	0.104
5	0.32 (cloudy)	0.47 (very cloudy)
6	0.052	0 22

from locality B. Quite divergent not only in volume, but also in uranium content, is the ratio between these two different parts of a crystal; and this seems to throw much light on the genesis of the zircon varieties in the granitic rocks.

Fusion of zircon

A minute zircon grain placed on a glass slide easily adheres to a heated NaF bead and, while xenotime and monazite melt and disperse into the bead in a few seconds, zircon shows much more

Table 3. Uranium migration into fused NaF bead.

Sample	Colour of zircon	Size of zircon	Approximate weight	Weight of NaF bead after the first fusion	Uranium migration (rough estimate from one grain of zircon)		
					First 1 minute fusion	Second* 1 minute fusion	Third* 3 minutes
(a)	Pale orange grey	$255\times168\times168\ \mu$	33.9×10^{-6} g	30.7 mg	4.82×10^{-3}	1.22×10^{-8}	1.59×10^{-8}
(b)	Greyish white	$382\times137\times137$	33.8	29.7	4.97×10^{-3}	6.3×10^{-10}	——
(c)	Brown	$274\times105\times105$	14.2	25.7	6.09×10^{-3}	1.63×10^{-9}	——
(d)	Yellow	$255\times105\times105$	13.7	40.3	8.45×10^{-3}	1.46×10^{-10}	——
(e)	Pale orange	$274\times94\times94$	12.2	36.3	4.95×10^{-3}	2.5×10^{-10}	3.35×10^{-10}

* Each residue was washed with water, fixed up upon a new NaF bead, and after one minute fusion given to the fluorescent test for the second time; the same process was repeated once more, but in the third time the fusion lasted three minutes.

resistance against the fusion. Before the zircon grain is completely melted, the uranium migration into the bead takes place, and the fluorescent light is fully seen. Five grains abundant in uranium content gave the result as shown in Table 3. In case of smaller grains, whose basal section is about $(0.1\ \text{mm})^2$ almost perfect uranium diffusion ends within a minute, though they still retain their skeletons inside the beads. In larger crystals, whose basal section is some $(0.15\ \text{mm})^2$ three minutes are required at least for the perfect diffusion,—about 75 per cent in the first one minute, some 19 per cent in the second one minute, and the remaining 6 per cent in the last one minute. (The heating conditions of the bead must be taken into consideration.) Whether cloudy or transparent, any zircon grain heated only one minute with NaF bead,

when the bead is washed away with water, leaves behind its porous and fragile skeleton; and this fragility is perhaps due to the ZrO_2 constituting the skeleton, since the NaF of the bead is combined with the SiO_2 formerly contained in the grain.

The homogeneous uranium density throughout the bead is ascertained by the fact that every part of the bead gives the same order of fluorescence.

Dilute HCl extraction of uranium

In case of the colourless and the transparent groups, the immersion of the crystals into dilute HCl brings forth no visible change in colour. In case of grains covered with coloured microfissures, however, the longer the immersion is, the more fading they undergo. The result of uranium fraction solved in the dilute HCl indicated, by the fluorescent method, is shown in Table 4. Probably no more

Table 4. Extraction of uranium from zircon grains by dilute HCl.

Locality	Number of zircon grains	Colour of zircon	Immersing time	Amount of uranium extracted from one grain
C	20	Cream, microfissures	20 day	0.4×10^{-10}
C	20	Brownish stain, microfissures	20	1.9
C	20	Brownish red, microfissures	20	10
C	4	Brownish red transparent	20	1
B	3	Dark brown soft*	20	163
A	15	Yellowish stain, microfissures	1	2.7

* It may be another mineral.

than only one per cent of uranium formerly contained in zircon grains is, indeed, soluble into the dilute HCl, but what is diffusible is not uranium alone. The disintegration products such as radium

and polonium, though not yet tested, seem also soluble into dilute acids.[8] The leaching test made by Hurley[3] on the extraction of radioactive elements contained in pulverized granite by means of dilute HCl seems to have been a similar case.

Alpha radioactivity of zircon by means of autoradiography

By the autoradiographic method, it is already clear that minute zircons contained in the Kitashirakawa granite leave, after 28 days exposure, their alpha tracks distinctly on the nuclear plates (ET-2E, 50 μ in thickness, Fuji Photo Film Co. Ltd.). Their size, alpha radioactivity and uranium equivalent are given in Table 5. Because the pleochroic haloes found around the zircon grains are RaC′ or RaA rings, uranium is the sole or nearly sole radioactive element which minute zircons enclose.*

It is true, indeed, that some unfavourable conditions, such as the diversity of the grain size, the wide range of their radioactivity, the friction fogging and others may be expected. Moreover, except the two samples K9a and K9b, all the zircon grains in the thin section are not listed in Table 5. All the zircon grains given in Table 5 belong to the highly radioactive group, for the weakly radioactive transparent group involving less than 0.02 per cent uranium can not be detected with nuclear emulsion in 28 days exposure, unless they are relatively large in size. In frequency, grains contained in a thin section of fresh granite are much different from those obtained out of pulverized rock.

While the fluorescent method is inapplicable to any grain under about 150 μ in length, the autoradiographic one can be applied to grains even under 100 μ in length. In case of zircons involving over 0.1 per cent uranium, however, the two different methods show a similar frequency.

* If the thorium content is negligibly small, from the track population $T\alpha = \psi\,(25.73U + 7.80Th)$ (Yagoda 1948)[9] and alpha permeability of zircon $\psi = 6.96$ (von Buttler 1951),[1] the uranium equivalent: $U = T\alpha/179$.

Table 5. Alpha radioactivity of minute zircon using nuclear emulsion.

Sample No.	Size (0.01 mm²)	$T\alpha$	Uranium equivalent
K28	0.16	0.84	0.47 per cent*
K27	0.26+0.25	0.13	0.63
K25	0.41	0.14	0.08
	0.19	0.72	0.40
K24	0.98	0.38	0.21
	0.34	0.31	0.17
	0.34	1.33	0.74
K19	0.92	0.14	0.08
	0.11	2.03	1.14*
K15	0.14	0.91	0.51*
	0 98	0.39	0.22
	0.36	0.78	0.44
K7	0.36	0.72	0.40
	0.85	0.22	0.12
	0.54	0.23	0.13
K5	0.30	0.19	0.11
K1	0.31	0.36	0.20
K9 (a)	0.10	2.19	1.22
	0.08	1.55	0.87*
	0.93	0.22	0.12
	0.22	0.39	0.22
	0.42	0.21	0.12
	0.08	2.81	1.57
	0.14	0.50	0.28
	0.25	0.18	0.10
	0.25	0.20	0.11
	0.32	0.30	0.17
	0.30	0.10	0.06
	0.25	0.40	0.22
K9 (b)	0.09	2.37	1.33**
	0.06	2.40	1.34**
	0.22	0.67	0.38
	0 20	0.88	0.49
	0.10	2.56	1.43
	0.06	3.44	1.92**
	0.21	2.81	1.57
	0.82	0.35	0.20
	0.05	2.07	1.16
	0.05	3.02	1.69
	0.02	1 88	1.05

* RaC′ halo in the biotite. ** In hornfelsic part.

From the petrographic view point, the wide range of the radioactivity of the accessory minerals seems to have been due to albitic deuteric actions, for, as it is clear under the microscope, the thin section of the granite is traversed by some narrow albite veinlets, and it is the most note-worthy fact that the zircon grains lying in the same veinlet show always the same degree of radioactivity.[2)]

Uranium content of zircons and their petrological meaning

According to Hutton's detailed study[4)] on detrital zircon, the transparent normal zircon shows feeble radioactivity, while the cloudy one gives high activity. The same tendency was seen also in the granitic rocks of various localities from the inner zone of the South Western part of Japan. On the other hand, von Buttler[1)] studied the heterogeneous distribution of radioactive elements in zircon and monazite obtained from pegmatite, and reduced it to the different stages of deposition of these elements. According to my autoradiographic studies, such a heterogeneity is seen in all other radioactive minerals. The stage of the growth of zircon crystal and that of uranium deposition in it seem, as the results of this paper suggest, to have belonged to different stages, even if both were the same deuteric. We may expect, however, as in case of the NaF bead, that the volatile substances, which could bring uranium into zircon in granitic rock, could possibly wash it away from the grain. Zircon which is cloudy but not abundant in radioactive elements, seems to have much of its content carried away by the volatile substances.

Conclusion and summary

1) The uranium content of each minute zircon grain is measurable by the fluorescent method easily and with greater precision.

2) Zircon grains obtained from the Kitashirakawa granite, though divergent in uranium content, can be reduced into two different

groups.

3) The colourless and transparent group is in general feebly radioactive (0.02~0.03 per cent uranium).

4) Grains covered with microfissures, coloured or colourless, is rich in uranium (0.1~0.7 per cent uranium).

5) As a rule, the colour of zircon has nothing to do with its uranium content.

6) The albite veinlets running through granite suggest the mechanism in which uranium was deposited in zircon grains.

Acknowledgements

The author expresses his hearty thanks to Prof. A. Harumoto for his valuable help and advice in carrying out this work. The cost of this investigation has been partly defrayed by the Scientific Grant of the Ministry of Education and by the Grant of the Hattori Hôkôkai, to which the author wishes to express his thanks.

References

1) von Buttlar, H. und F. G. Houtermans: Geochim. Cosmochim. Acta, **2**, 43 (1951).
2) Hayase, I.: Mem. Coll. Sci. Univ. Kyoto, Ser. B, **20**, No. 4, 247 (1953).
3) Hurley, P. M.: Bull. Geol. Soc. Amer., **61**, 1 (1950).
4) Hutton, C. O.: Bull. Geol. Soc. Amer., **61**, 636 (1950).
5) Nakanishi, M.: Bull. Chem. Soc. Japan, **24**, 33 (1951).
6) Northup, M. A.: Ind. Eng. Chem., Anal. Ed., **17**, 664 (1945).
7) Shibata, Y.: Uranium (Tokyo, Maruzen, 1953, in Japanese), 49; 81.
8) Starik, I. Je.: Chem. Zentr., 1555 (1938).
9) Yagoda, H.: Radioactive measurements with nuclear emulsion (New York, John Wiley, 1949), 163.

Manuscript received July 26, 1954.

MINERALOGICAL JOURNAL, VOL. 1, NO. 3, PP. 160-169, OCT., 1954

THE CRYSTAL STRUCTURE OF ORPIMENT (As_2S_3) REFINED

NOBUO MORIMOTO

Mineralogical Institute, University of Tokyo

ABSTRACT

The crystal structure of orpiment, As_2S_3, was refined by the Fourier synthesis. The unit cell has the dimensions, $a=11.46$ Å, $b=9.57$ Å, $c=4.22$ Å and $\beta=90.5°$, containing four As_2S_3. The space group is $C_{2h}^5-P2_1/n$. The structure is essentially the same as one described earlier.

Introduction

In the original analysis of orpiment, the usual trial-and-error method was used[7]. The crystal structure of realgar determined subsequently by the inequality relations and Fourier synthesis is considered much more precise. The relationship between these two related minerals has been discussed already[6].

The present study was undertaken in order to refine the atomic parameters of orpiment by means of the Fourier analysis, so that our discussion might be based on much more balanced data.

Experimental

Many experimental data were added to those used earlier. The specimens examined were the crystals from Saimoku, Japan[5]. The Weissenberg photographs were taken about the *a*, *b* and *c* axes by the multiple technique (Co $K\alpha$ radiation (1.79 Å)).

The relative intensities were estimated visually correcting for the Lorentz and polarization factors. No absorption correction was applied because of the difficulty due to the irregular shape of the

samples used. The effect of absorption, however, was reduced to minimum by comparing the relative intensity of a number of identical reflections from different samples.

The relative intensities were converted into the absolute ones by the method of Harker[4]. They were multiplied by a proportionality factor that minimized the sum of a certain number of the differences $||F_o|-|F_c||$.

The unit cell has the dimensions, $a=11.46\pm0.04$ Å, $b=9.57\pm0.02$ Å, $c=4.22\pm0.05$ Å and $\beta=90.5\pm0.5°$, containing four As_2S_3. The space group is $C_{2h}^5-P2_1/n$ with reflexions $h0l$ and $0k0$ absent respectively when $h+l$ and k are odd.[2]

Refinement by the Fourier synthesis

For summation the Beever-Lipson strips were used. The a and b axes were divided into 60 parts each with intervals of 0.19 and 0.16 Å, and the c axis into 30 parts with intervals of 0.14 Å.

The first summation of xy synthesis was carried out using 77 observed F_{hk0}'s whose signs were determined with certainity by the atomic parameters obtained in the previous study. The second summation was made with 91, and the third with 94 terms (all including zero terms), making successive adjustment of atomic positions. The xz synthesis was made in a similar way, the first one with 35, the second with 40, and the third with 41 terms (all including zero terms). In these syntheses, the effect of cutting off the higher-order Fourier terms was minimized by the method of Cochran.[3]

The final Fourier diagrams of electron density projected on (001) and (010) planes are given in Fig. 1. In these the maxima of contours of all the atoms in the cell are clearly resolved to read off immediately their parameters, excepting the z parameters of two of the sulfur atoms which overlap in the (010) projection. These were determined by a graphical method.[6]

The coordinates of atoms finally determined are given in Table 1,

Fig. 1. Fourier projections of electron density on (a) (001) and (b) (010). Contours at intervals of 10 e. Å^{-2}, the zero-electron lines being broken.

Table 1. Coordinates of atoms

Atom	No. of atoms in the cell	*x/a*		*y/b*		*z/c*	
		(1)	(2)	(1)	(2)	(1)	(2)
As_1	4	.268	.267	.187	.190	.161	.143
As_2	4	.482	.484	.313	.323	.664	.643
S_1	4	.410	.395	.120	.120	.454	.500
S_2	4	.340	.355	.380	.397	−.046	.013
S_3	4	.125	.125	.305	.293	.455	.410

(1) Values by the previous study
(2) Final values by this study

compared with the original ones. Probable errors were estimated by the method of Booth[1] to be 0.04 Å for sulfur atoms and 0.02 Å for arsenic atoms. In Table 2, the structure factors calculated on the basis of the refined structure are given as also those experimentally determined. The reliability factor, $R=\Sigma||F_o|-|F_c||\div\Sigma|F_o|$, is 0.15 for *hk*0 reflexions, 0.21 for *h*0*l* reflexions, and 0.18 for *hkl* reflexions, all present and absent reflexions being counted.

The structure redescribed

The refined structure of orpiment as illustrated in Fig. 2, which like Fig. 1 is projected on (001) and (010) planes, is essentially the same as one originally described except for a few shifts in atomic positions which considerably improved the interatomic distances and the atomic bond angles.

The structure consists of As_2S_3 layers, in which spiral chains, AsS, running parallel to the *c* axis, can be seen (Fig. 3). The layers are parallel to (010) and held together by the van der Waals force.

In the structure, each arsenic atom is surrounded by three sulfur atoms and each sulfur atom is shared by two arsenic atoms. The covalent bond distances and the bond angles are given in Table 3. The mean value of the covalent bond distances between arsenic and

Table 2. Comparison of observed and calculated F-values

hkl	sin θ	F_{obs}	F_{calc}	*hkl*	sin θ	F_{obs}	F_{calc}	*hkl*	sin θ	F_{obs}	F_{calc}
200	.156	–	2.8	630	.546	91	90.8	560	.686	40	39.2
400	.312	63	67.8	730	.615	114	−103.2	660	.733	–	4.8
600	.468	–	− 0.8	830	.685	11	− 15.2	760	.786	–	0.8
800	.625	157	173.2	930	.756	42	48.4	860	.842	90	68.4
10.00	.781	–	7.2	10.30	.830	4	0.4	960	.903	22	18.0
				11.30	.906	65	− 72.4	10.60	.959	40	26.4
210	.182	72	− 62.4								
310	.252	38	49.2	040	.377	78	− 77.2	170	.664	–	13.6
410	.326	–	− 3.2	140	.384	74	− 75.6	270	.674	37	39.2
510	.411	56	49.2	240	.407	27	− 30.4	370	.696	10	− 14.4
610	.478	84	− 92.4	340	.443	135	133.4	470	.730	–	− 3.6
710	.564	72	71.2	440	.489	29	27.2				
810	.631	–	− 4.4	540	.543	45	− 35.6	080	.744	107	−102.8
910	.710	29	− 38.6	640	.601	17	− 18.4	180	.756	21	22.0
10.10	.786	74	− 88.8	740	.664	78	72.4	280	.768	–	11.6
11.10	.865	–	9.6	840	.729	10	26.0	380	.789	21	2.4
				940	.796	–	12.8	480	.815	152	−131.2
020	.188	203	−185.6	10.40	.865	40	− 13.3	580	.843	72	− 62.8
120	.204	29	42.4					680	.881	–	6.8
220	.244	–	9.2	150	.471	31	31.6				
320	.300	94	− 86.8	250	.497	52	49.2	190	.850	70	− 53.2
420	.364	106	− 96.8	350	.526	138	130.8	290	.860	–	− 2.4
520	.434	72	63.2	450	.564	14	22.4	390	.879	57	− 56.0
620	.505	14	14.4	550	.612	14	16.4	490	.901	40	− 33.2
720	.578	113	−104.8	650	.664	14	17.6				
820	.653	104	− 88.8	750	.722	47	34.2	101	.209	61	− 64.0
920	.728	51	− 65.2	850	.781	–	− 2.4	301	.314	202	217.6
10.20	.803	–	− 7.6	950	.841	10	− 10.8	501	.425	–	3.6
11.20	.879	40	− 34.0	10.50	.902	46	61.6	701	.587	108	113.6
								901	.726	26	9.2
130	.294	52	− 53.2	060	.564	102	96.4	11.01	.883	178	156.8
230	.322	87	− 90.8	160	.570	31	28.4				
330	.367	135	−137.2	260	.586	23	27.2	002	.425	67	54.0
430	.412	–	− 8.0	360	.612	117	116.2	202	.452	45	78.8
530	.481	100	− 77.6	460	.646	138	132.0	402	.527	132	−109.6

Table 2.—*Continued*

hkl	sin θ	F_{obs}	F_{calc}	*hkl*	sin θ	F_{obs}	F_{calc}	*hkl*	sin θ	F_{obs}	F_{calc}
602	.631	69	48.4	511	.455	38	30.0	241	.460	–	20.8
802	.757	22	22.8	611	.524	27	28.8	341	.492	16	– 23.6
10.02	.890	144	131.8	711	.595	84	76.0	441	.533	141	–142.4
				811	.666	14	6.0	541	.582	24	19.2
103	.640	107	–107.6	911	.740	–	2.0	641	.636	51	60.4
303	.680	41	– 59.2	10.11	.815	40	44.8	741	.696	16	14.0
503	.748	41	– 36.8	11.11	.890	34	– 33.2	841	.760	54	– 47.6
703	.840	89	50.0					941	.827	60	– 68.8
				021	.284	90	67.2	10.41	.894	44	51.6
004	.851	56	– 77.2	121	.293	46	53.6				
				221	.324	93	93.2	051	.516	160	186.4
$10\bar{1}$	.209	124	144.0	321	.368	111	–115.6	151	.523	40	– 31.6
$30\bar{1}$	.316	38	54.8	421	.422	114	112.8	251	.540	19	41.6
$50\bar{1}$	.425	29	23.2	521	.482	29	– 17.6	351	.569	–	– 11.6
$70\bar{1}$	.587	103	– 84.8	621	.547	94	–104.4	451	.604	–	– 12.8
$90\bar{1}$	.726	28	11.2	721	.615	118	–110.4	551	.650	19	– 20.8
$11.0\bar{1}$	.883	66	50.0	821	.685	45	41.6	651	.699	37	33.5
				921	.758	32	36.0	751	.752	27	– 21.6
$20\bar{2}$	.452	55	– 75.2	10.21	.830	27	– 16.0	851	.811	66	90.8
$40\bar{2}$	.527	95	–116.8	11.21	.907	56	– 70.4	951	.872	12	2.0
$60\bar{2}$	.631	79	– 55.2								
$80\bar{2}$	.757	39	25.6	031	.353	106	–102.0	061	.604	59	53.2
$10.0\bar{2}$	.890	156	–130.0	131	.362	12	– 0.8	161	.599	16	18.4
				231	.386	29	– 46.8	261	.624	51	– 60.4
$10\bar{3}$	.640	–	7.6	331	.424	–	24.4	361	.641	78	83.2
$30\bar{3}$	.680	64	– 83.2	431	.471	102	–107.6	461	.681	86	79.6
$50\bar{3}$	.748	40	– 66.4	531	.526	44	– 44.0	561	.720	26	17.6
$70\bar{3}$	.840	162	–165.6	631	.586	46	– 64.4	661	.766	43	– 32.0
				731	.652	11	8.4	761	.815	93	123.6
$20\bar{4}$	.864	–	– 19.2	831	.716	60	– 58.4	861	.870	52	41.2
$40\bar{4}$	.902	114	–126.2	931	.788	36	45.4				
				10.31	.859	59	– 89.6	071	.693	47	– 55.2
211	.280	23	23.2					171	.698	54	46.8
311	.330	38	– 38.0	041	.432	135	–125.2	271	.711	–	– 2.8
411	.389	55	93.6	141	.445	43	– 48.4	371	.731	24	18.0

Table 2.—*Continued*

hkl	sin θ	F_{obs}	F_{calc}	*khl*	sin θ	F_{obs}	F_{calc}	*kkl*	sin θ	F_{obs}	F_{calc}
471	.759	17	27.6	52$\bar{1}$	.482	87	− 42.4	55$\bar{1}$	.650	43	34.4
571	.795	66	59.6	62$\bar{1}$	.547	126	−115.2	65$\bar{1}$	.699	57	− 42.0
671	.839	50	35.2	72$\bar{1}$	.615	25	28.2	75$\bar{1}$	.752	60	50.4
771	.882	12	1.6	82$\bar{1}$	.685	58	− 51.6	85$\bar{1}$	.811	111	108.0
				92$\bar{1}$	.758	28	26.4	95$\bar{1}$	.872	12	7.6
081	.782	32	35.6	10.2$\bar{1}$	.830	53	− 28.0				
181	.788	48	46.0					16$\bar{1}$	.599	78	82.0
281	.800	21	− 24.4	13$\bar{1}$	.362	30	28.0	26$\bar{1}$	.624	11	− 13.2
381	.819	93	−110.4	23$\bar{1}$	.386	39	42.0	36$\bar{1}$	.641	15	− 19.6
481	.846	−	0.8	33$\bar{1}$	.424	46	40.8	46$\bar{1}$	.681	63	− 71.2
581	.875	46	− 26.8	43$\bar{1}$	.471	100	−104.0	56$\bar{1}$	.720	31	31.6
681	.910	56	58.4	53$\bar{1}$	.526	74	− 71.2	66$\bar{1}$	.766	14	− 3.2
				63$\bar{1}$	.586	42	46.0	76$\bar{1}$	.815	16	12.4
091	.873	58	− 76.4	73$\bar{1}$	.652	60	69.3	86$\bar{1}$	.870	23	− 7.2
191	.889	60	− 41.6	83$\bar{1}$	.716	75	− 59.2				
291	.909	19	− 25.2	93$\bar{1}$	.788	47	36.8	17$\bar{1}$	.698	40	− 35.6
391	.929	24	4.0	10.3$\bar{1}$	.859	87	92.8	27$\bar{1}$	.711	34	38.6
								37$\bar{1}$	.731	99	−104.8
21$\bar{1}$	.280	14	− 12.0	14$\bar{1}$	.445	37	− 26.0	47$\bar{1}$	.759	−	6.4
31$\bar{1}$	.330	150	−196.0	24$\bar{1}$	.460	15	14.8	57$\bar{1}$	.795	34	22.8
41$\bar{1}$	.389	84	87.2	34$\bar{1}$	.490	12	− 9.6	67$\bar{1}$	.839	53	28.8
51$\bar{1}$	.455	−	14.8	44$\bar{1}$	.533	122	122.8	77$\bar{1}$	.882	138	−142.8
61$\bar{1}$	.524	25	− 18.0	54$\bar{1}$	.582	44	34.8				
71$\bar{1}$	.595	121	−105.2	64$\bar{1}$	.636	65	63.6	18$\bar{1}$	.788	62	− 55.6
81$\bar{1}$	.666	28	6.0	74$\bar{1}$	.696	31	15.2	28$\bar{1}$	.800	85	− 88.0
91$\bar{1}$	.740	−	0.4	84$\bar{1}$	.760	85	68.0	38$\bar{1}$	.819	−	0.4
10.1$\bar{1}$	.815	27	− 34.0	94$\bar{1}$	.827	54	− 38.0	48$\bar{1}$	.846	−	− 5.2
11.1$\bar{1}$	.890	170	−140.0	10.4$\bar{1}$	.894	51	50.0	58$\bar{1}$	.875	69	− 61.2
								68$\bar{1}$	.910	16	8.0
12$\bar{1}$	.293	61	− 86.8	15$\bar{1}$	.523	35	30.8				
22$\bar{1}$	.324	71	74.4	25$\bar{1}$	.540	61	− 55.2	19$\bar{1}$	.889	11	− 11.6
32$\bar{1}$	.368	−	− 7.6	35$\bar{1}$	.569	80	86.4	29$\bar{1}$	.909	19	− 18.8
42$\bar{1}$	.422	117	112.6	45$\bar{1}$	.604	14	0.8	39$\bar{1}$	.929	57	71.6

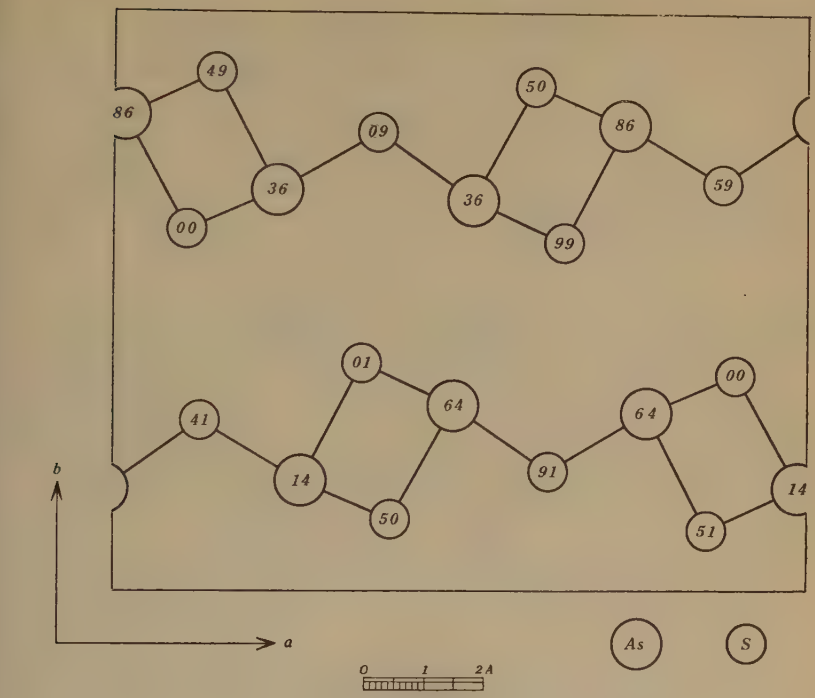

Fig. 2. The structure of orpiment, projected on (a) (001) and (b) (010). (The figure corresponds to Fig. 1). Numbers give the height of each atom in the cell expressed as a percentage of the *c* and *b* translation.

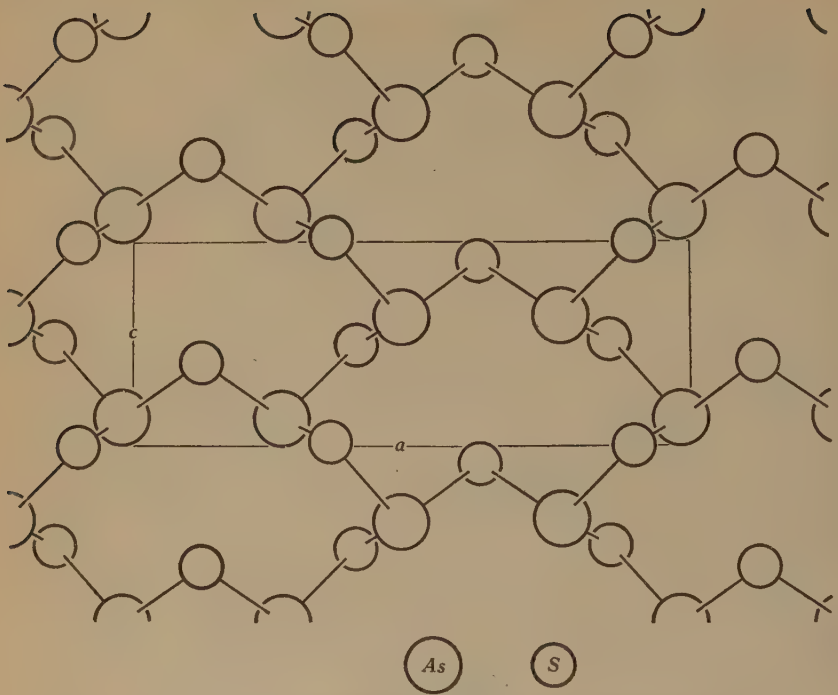

Fig. 3. The layer in the orpiment structure (projected on (010)). The spiral chains, AsS, composing the layer are to be seen.

Table 3. Interatomic distances and bond angles

1. Covalent bond distances (Å)

As_1-S_1	2.21	As_2-S_1	2.26
As_1-S_2	2.28	As_2-S_2	2.26
As_1-S_3	2.22	As_2-S_3	2.23

2. Bond angles (°)*

$\angle As_1-S_1-As_2$	102.8	$\angle S_1-As_1-S_2$	97.1
$\angle As_1-S_2-As_2$	100.6	$\angle S_2-As_1-S_3$	94.5
$\angle As_1-S_3-As_2$	94.4	$\angle S_3-As_1-S_1$	106.5
		$\angle S_1-As_2-S_2$	95.2
		$\angle S_2-As_2-S_3$	106.1
		$\angle S_3-As_2-S_1$	92.7

* Bond angles obtained by construction

3. Non-bonded distances (Å)

As_1-As_2	3.25	S_1-S_2	3.36
	3.49		3.36
	3.49	S_2-S_3	3.30
			3.58
		S_3-S_1	3.55
			3.24

sulfur atoms is 2.24 Å, and the mean values of the bond angles ∠As–S–As and of ∠S–As–S are respectively 99.3° and 98.7°.

The highly perfect cleavage of orpiment after (010) is parallel to the As_2S_3 layers.

It is interesting to note that the bond angles of the sulfur atoms added in between the spiral chains differ from those of the sulfur atoms in the chains. This would mean that the former sulfur atoms play a different role from the latter in the orpiment structure.

In conclusion the writer wishes to express his sincere thanks to Prof. Ito for suggestion and guidance throughout the work.

References

1) Booth, A. D.: Fourier Technique in Organic Structure Analysis. (Cambridge, University Press, 1948).
2) Buerger, M. J.: Amer. Miner., 27, 301 (1942).
3) Cochran, W.: Acta Cryst., 1, 138 (1948).
4) Harker, D.: Amer. Miner., 33, 764 (1948).
5) Ito, T. and K. Sakurai: Wada's Minerals of Japan, 3rd Ed., 26 (1947).
6) Ito, T., N. Morimoto and R. Sadanaga: Acta Cryst., 5, 775 (1952).
7) Morimoto, N.: X-rays, 5, 115 (1949).

Manuscript received August 19, 1954.

MINERALOGICAL JOURNAL, VOL. 1, NO. 3, PP. 170-184, OCT., 1954

THE NUMBER OF COUNTS OF BETA-RAYS DETECTED BY AN END-WINDOW GEIGER-MUELLER COUNTER*

NOBUO KATAYAMA

Institute of Earth Science, College of General Education
University of Tokyo

ABSTRACT

The number of counts per minute of beta-rays detected by an end-window Geiger-Mueller counter is given by the following formula:

$$T = \frac{60\pi pNW}{C^*} \sum_n G_{(n,n+1)},$$

where p: the content of a beta-active isotope (in decimal).
N: the number of beta-rays emitted by the beta-active isotope per gram per second.
W: a term representing the absorption effect due to the substances between the sample and the sensitive volume of the counter.
C^*: the mass absorption coefficient for any substance regarding the number of the beta-rays. ($cm^2\ gr^{-1}$)
$\sum_n G_{(n,n+1)}$: calculated from the geometrical relation of apparatus and procedure as well as the absorption coefficient of the beta-ray for the sample. n: from 0 up to the value approximately enough for saturation.

Introduction

In the course of a study of the beta-rays of minerals and rocks the writer's attention was called to the possibility of calculating the number of counts of beta-rays detected by a Geiger-Mueller counter.

* Dedicated to Dr. S. Tusboi, Emeritus Professor of University of Tokyo, on the occasion of his sixtieth birthday.

A preliminary report was read at the Annual Meeting of the Japan Society of Analytical Chemistry, 1952, and a conclusive one, at the Annual Meeting of the Mineralogical Society of Japan on June 5, 1954.

The reports concerning this problem published already by E. Berne[1] and by G. B. Cook, J. F. Duncan and M. A. Hewitt[2] are all concerned with the geometrical efficiency of an end-window Geiger-Mueller counter. However, the number of counts could not be adequately calculated disregarding the absorption effect due to the sample itself. The writer has therefore tried to calculate it taking into account this effect too.

Effective solid angle

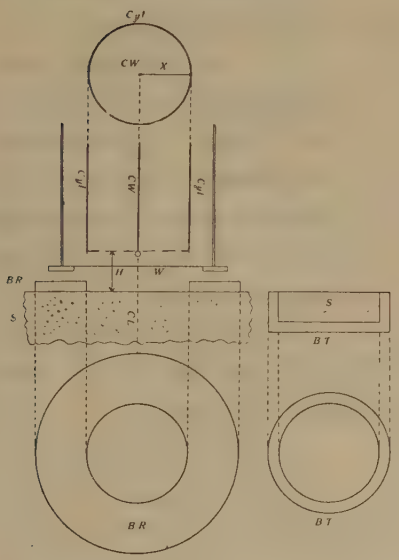

Fig. 1. Scheme of a mica-window beta counter with a sample.
CW: central wire. *Cyl*: cylinder cathode.
W: window. *CL*: central line.
S: sample. *BR*: brass ring.
BT: brass tray for powders.

Fig. 1 shows the geometrical relation of the apparatus usually used schematically. X denotes in cm. the radius of the cylinder cathode of the counter, and H the distance between the end point of the central wire and the center of the surface of the sample. The z axis is taken parallel to the central wire with the positive direction downward. The x axis is taken parallel to the surface of the sample. The origin of the coordinate is always taken on the central line.

Though the individual tracks of beta-rays might not be linear, we assume for simplicity that they are linear on the whole.

Among the beta-rays from the sample only those traversing the sensitive volume of the counter can be detected. If the source of

beta-ray is a point, the parts of rays with the tracks lying inside the cone, the vertex of which is the point source and the base the basal section of the sensitive volume, are effective.

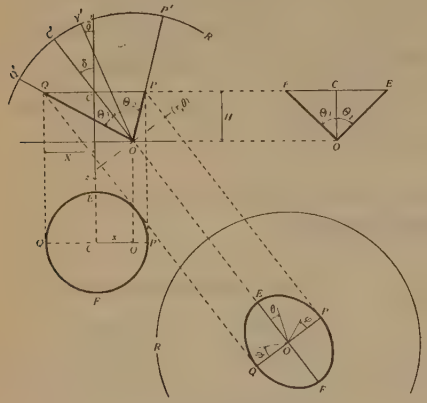

Fig. 2. Effective solid angle.
O : point source.
C : the end point of the central wire.
$PEQF$: the basal section of the sensitive volume.
R : an arbitrary sphere.

The ratio of the number of effective rays to the total number of beta-rays from the sample is equal to the solid angle of the cone. This solid angle is designated as "effective solid angle".

Fig. 2 shows the geometry in projection of the effective solid angle. O represents the point source; C the end point of the central wire; PEQF the base of the sensitive volume.

Let r and θ be polar coordinates in the plane (r, θ) which is perpendicular to OC. Then the solid angle S is given by the following formula:

$$S=\frac{R\iint_A \frac{r}{\sqrt{R^2-r^2}}\,drd\theta}{4\pi R^2}=\frac{1}{2\pi}\left[\pi-\left\{\int_{-\frac{\pi}{6}}^{\frac{\pi}{6}} F_1(\theta)d\theta+\int_0^{\frac{\pi}{3}} F_2(\varphi)d\varphi+\int_0^{\frac{\pi}{3}} F_3(\psi)d\psi\right\}\right], \qquad (1)$$

where

$$F_1(\theta)=\sqrt{\frac{p^2\cos^2\delta+(X^2+p^2)\sin^2\delta\sin^2\theta-2xX\sin\theta_1}{(X^2+p^2)\cos^2\delta+(X^2+p^2)\sin^2\delta\sin^2\theta-2xX\sin\theta}}\Big/\sqrt{\frac{\cos^2\delta+\sin^2\delta\sin^2\theta}{\cos^2\delta+\sin^2\delta\sin^2\theta}};$$

$$F_2(\varphi)=\sqrt{\frac{p^2\cos^2\delta+(X^2+p^2)\sin^2\delta\cos^2\varphi-2xX\cos\varphi_1}{(X^2+p^2)\cos^2\delta+(X^2+p^2)\sin^2\delta\cos^2\varphi-2xX\cos\varphi}}\Big/\sqrt{\frac{\cos^2\delta+\sin^2\cos^2\varphi}{\cos^2\delta+\sin^2\cos^2\varphi}};$$

$$F_3(\psi)$$

$$=\sqrt{\frac{p^2\cos^2\delta+(X^2+p^2)\sin^2\delta\cos^2\psi+2xX\cos\psi\sqrt{\cos^2\delta+\sin^2\delta\cos^2\psi}}{(X^2+p^2)\cos^2\delta+(X^2+p^2)\sin^2\delta\cos^2\psi+2xX\cos\psi\sqrt{\cos^2\delta+\sin^2\delta\cos^2\psi}}};$$

$$p^2=OC^2=H^2+x^2;$$

$$\delta=\angle OCZ,\quad \sin\delta=\frac{x}{p};$$

R: the radius of an arbitrary sphere.

Expanding the functions $F_1(\theta)$, $F_2(\varphi)$ and $F_3(\psi)$ by Maclaurin's Theorem, we obtain the following equality:

$$S=\frac{1}{2\pi}\left[\pi-\frac{1}{3}\left\{F_1(0)+F_2(0)+F_3(0)\right\}\pi+\left\{\frac{F_1''(0)}{648}+\frac{F_3''(0)}{162}\right\}\pi^3+\frac{F_3'''(0)}{1940}\pi^4+\cdots\right].$$

In our experiments we have put $X=1$, $x=0\sim1$ and $p=1\sim\sqrt{2}$. In this case, regarding the results of numerical calculation, the preceding equality, allowing the error less than one per cent, may be simplified as follows:

$$S=\frac{1}{2}\left[1-\frac{1}{3}\left\{F_1(0)+F_2(0)+F_3(0)\right\}\right], \tag{2}$$

where
$$F_1(0)=\frac{p}{\sqrt{X^2+p^2}}; \tag{3-1}$$

$$F_2(0)=\frac{p-X\sin\delta}{\sqrt{X^2+p^2-2xX}}; \tag{3-2}$$

$$F_3(0)=\frac{p+X\sin\delta}{\sqrt{X^2+p^2+2xX}}. \tag{3-3}$$

If we define the angles Θ_1, Θ_2 and Θ_3 as shown in Fig. 2, these $F_1(0)$, $F_2(0)$ and $F_3(0)$ are no other than $\cos\Theta_1$, $\cos\Theta_2$ and $\cos\Theta_3$ respectively. Further it is convenient to define an angle β such

$$\cos\beta=\frac{\cos\Theta_1+\cos\Theta_2+\cos\Theta_3}{3}. \tag{4}$$

By using the angle β, equality (2) becomes

$$S=\frac{1-\cos\beta}{2}. \tag{5}$$

This equality means that β is the semi-angle of a right cone, the solid angle of which being equal to that of the cone O–PEQF. If the vertex of this right cone is set to O and its axis is orientated in such a way that it devides the angle POQ symmetrically, the right cone will nearly coincide in position with the cone O–PEQF, so that the effective solid angle hereafter is represented by the right cone.

Fig. 3 shows the relation by stereographic projection. In Fig. 3, the thin line P′E′Q′F′ represents the solid angle of the cone O–PEQF and the thick line, that of the right cone with the semi-angle β. OC and the axis of the right cone meet the sphere in the points C′ and Y′ respectively.

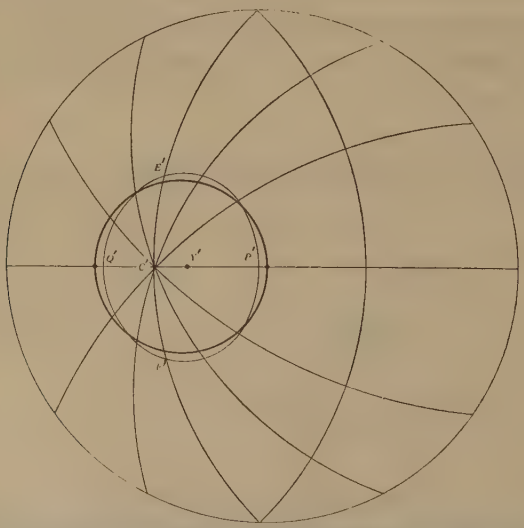

Fig. 3. Stereographic projection of an effective solid angle.
$P'E'Q'F'$: effective solid angle.
Thick line: the solid angle of the right cone with the semi-angle β.
C': the point in which OC meets the sphere.
Y': the point in which the axis of the right cone meets the sphere.

Mean declination of tracks

The absorption of beta-ray by a medium relates to the length of their tracks in it, which is the function of the angle of declination of each track. For simplicity we calculate the mean declination of the tracks of the beta-rays contained within the effective solid angle.

Let r' and θ' be polar coordinates in the plane (r', θ') which is perpendicular to the axis of the right cone. Then, the mean declination D is given by

$$\cos D = \frac{\iint_A \cos\rho \frac{Rr'}{\sqrt{R^2-r'^2}}\, dr'd\theta'}{\iint_A \frac{Rr'}{\sqrt{R^2-r'^2}}\, dr'd\theta'}, \tag{6}$$

where R denotes the radius of an arbitrary sphere, ρ the declination of track given by

$$\cos\rho = \frac{\sqrt{R^2-r'^2}}{R}\cos\delta' + \frac{r'}{R}\sin\delta'\cos\theta',$$

and δ' the angle between the axis of the right cone and the central line (see Fig. 2) given by

$$\delta' = \frac{1}{2}\left\{\tan^{-1}\left(\frac{X+x}{H}\right) - \tan^{-1}\left(\frac{X-x}{H}\right)\right\}.$$

Integration of the numerator of equality (6) follows:

$$\iint_A \cos\rho \frac{Rr'}{\sqrt{R^2-r'^2}}\, dr'd\theta' = 2\int_0^{\pi}\left\{\int_0^{R\sin\beta}\cos\rho\, \frac{Rr'}{\sqrt{R^2-r'^2}}\, dr'\right\} d\theta'$$

$$= \pi R^2\cos\delta'\sin^2\beta + 2R^2\sin\delta'(\beta - \sin\beta\cos\beta);$$

hence $$\cos D = \frac{\pi\cos\delta'\sin^2\beta + 2\sin\delta'(\beta-\sin\beta\cos\beta)}{2\pi(1-\cos\beta)} \tag{7}$$

Differential of the number of effective beta-rays

The differential dU of the number of effective beta-rays per second is given by the following equality,

$$dU=2\pi x\cdot dx\cdot dz\cdot \rho^* pNS, \tag{8}$$

where ρ^* denotes the apparent density of the sample, p the content of the beta-active isotope in the sample in decimal, and N the number of beta-rays from the isotope per second per gram.

Introducing the absorption coefficient μ^*, if the content of the beta-active isotope is homogeneous throughout the sample equality (8) becomes,

$$dU_{z_1}=2\pi x dx\rho^* pN\int_0^{z_1} Se^{-\frac{\mu^* z}{\cos D}}dz. \tag{9}$$

Here, we have taken into account the number, instead of intensity, of the beta-rays passing through the sample. We may, further, assume that U_z, the number of parallel beta-rays counted at the distance z from the source, is given by the following equality;

$$U_z=U_0 e^{-\mu^* z},$$

where U_0 denotes the number of the beta-rays emitted from the source. In the case of radial beta-rays, z must be substituted by $\frac{z}{\cos D}$, the mean length of the tracks of the beta-rays in the sample, as in equality (9). Cos D is a function of H, which, in regard to a particular sample, may be substituted by $H+z$, H being a constant. Hence, cos D is a function of z.

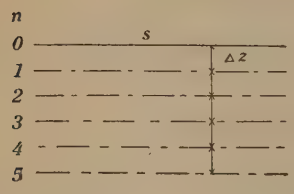

Fig. 4. Parallel layers Δz thick.
s: surface of the sample.
n: number of dividing plane.

In order to perform integration of equality (9), we consider the sample constituted from a number of parallel layers Δz cm. thick, assigning a suitable value to Δz so that cos D can be regarded practically as a constant between $H+n\Delta z$ and $H+(n+1)\Delta z$ (Fig. 4). Between the n-th dividing plane and the $(n+1)$-th plane of the layers, the integration follows:

$$\int_0^{\Delta z} Se^{-\frac{\mu^* z}{\cos D_{(n,n+1)}}} dz = \frac{\cos D_{(n,n+1)}}{2\mu^*} L_{(n,n+1)}, \qquad (10)$$

$$L_{(n,n+1)} = (1-\cos\beta_n) - e^{-\frac{\mu^* \Delta z}{\cos D_{(n,n+1)}}} (1-\cos\beta_{n+1})$$

$$- \frac{\cos D_{(n,n+1)}}{\mu^*} \left\{ F_n(0) - e^{-\frac{\mu^* \Delta z}{\cos D_{(n,n+1)}}} F_{n+1}(0) \right\}$$

$$- \left(\frac{\cos D_{(n,n+1)}}{\mu^*} \right)^2 \left\{ F'_n(0) - e^{-\frac{\mu^* \Delta z}{\cos D_{(n,n+1)}}} F'_{n+1}(0) \right\}, \qquad (11)$$

where $F(z) = \frac{\partial(\cos\beta)}{\partial z}$.

Number of the counts of beta-rays detected

The beta-rays from the $(n, n+1)$ layer within the effective solid angle, before they enter the sensitive volume, will be absorbed by the layers $(n-1, n)$, $(n-2, n-1)$, ... $(0, 1)$, $n\Delta z$ cm. thick, in addition to the window of the counter. With this absorption accounted, equalities (9) and (10) give for the differential dT of the number of counts per minute of the effective beta-rays from the $(n, n+1)$ layer:

$$dT_{(n,n+1)} = 60 \frac{\pi p N}{C^*} e^{-\frac{-\sigma C^*}{\cos D_{(n,n+1)}}} e^{-\frac{-\mu^* n \Delta z}{\cos D_{(n,n+1)}}} \cos D_{(n,n+1)} \cdot L_{(n,n+1)} x dx, \qquad (12)$$

where $C^* = \frac{\mu^*}{\rho^*}$ and may be assumed to be constant for a definite beta-ray, σ denotes the thickness of the window in gram per square centimeter.

When the sample is homogeneous, $\frac{\pi p N}{C^*}$ is a constant. σ being very small, a small variation of the value of cos D will not effect the value of $e^{-\frac{\sigma C^*}{\cos D_{(n,n+1)}}}$ more than one per cent. Hence the term

$e^{-\frac{\sigma C^*}{\cos D_{(n,n+1)}}}$ can be assumed to be constant approximately.

In addition to the absorption by the window, there are some other factors which reduce the number of beta-rays between the sample and the sensitive volume. The total sum of those effects and the absorption by the window may be expressed by a single term W, which may be regarded also as constant approximately unless experimental condition changes.

Integration of $dT_{(n,n+1)}$ follows:

$$T_{(n,n+1)}=60\frac{\pi pNW}{C^*}G_{(n,n+1)}, \tag{13}$$

$$G_{(n,n+1)}=\int_{x_1}^{x_2} e^{-\frac{\mu^* n\Delta z}{\cos D_{(n,n+1)}}}\cos D_{(n,n+1)}\,L_{(n,n+1)}\,x\,dx. \tag{14}$$

Hence, T, the total number per minute of the effective beta-rays is given by

$$T=60\frac{\pi pNW}{C^*}\sum_n G_{(n,n+1)}. \tag{15}$$

Since Geiger-Mueller counters have practically 100 per cent detection efficiency for beta-rays, T is no other than the number of the counts of beta-rays detected by the counter.

In equality (15), p is dependent solely on the nature of sample, N on that of the beta-active isotope in the sample, and W on the instrumental and experimental conditions. As for C^*, it may be assumed as a constant in regard to a definite beta-active isotope. $\Sigma G_{(n,n+1)}$ is calculated from the geometrical relations of the apparatus and the procedure as well as the absorption coefficient of the beta-ray for the sample.

Suitable value for Δz

In order to determine a suitable value for Δz, the values of $\cos D$ at various points were calculated from equality (7) and the results

are tubulated in Table 1, where the values of cos D at x=0, 0.1, 0.2.....0.9, 1.0 cm. on each n-th plane with Δz=0.05 cm. are shown. As is evident in Table 1, if we designate cos $D_{(n,n+1)}$ in regard to a definite value of x by

$$\cos D_{(n,n+1)} = \frac{\cos D_n + \cos D_{n+1}}{2}, \qquad (16)$$

the values of cos D in the $(n, n+1)$ layer do not deviate from the value of cos $D_{(n,n+1)}$ more than one per cent. Hence 0.05 cm. is a suitable value for Δz.

Table 1. The values of cos D_n
X=1.00 cm., H=0.80 cm., Δz=0.05 cm..

x cm	cos D_0	cos D_1	cos D_2	cos D_3	cos D_4	cos D_5	cos D_6
0	0.81$_2$	0.82$_3$	0.83$_6$	0.84$_2$	0.85$_3$	0.86$_1$	0.87$_0$
0.1	0.82$_9$	0.84$_1$	0.84$_6$	0.86$_0$	0.86$_3$	0.87$_8$	0.88$_3$
0.2	0.84$_5$	0.85$_7$	0.86$_3$	0.87$_5$	0.88$_3$	0.88$_8$	0.90$_1$
0.3	0.85$_9$	0.87$_3$	0.87$_5$	0.88$_7$	0.88$_7$	0.90$_4$	0.91$_1$
0.4	0.87$_2$	0.88$_3$	0.89$_7$	0.89$_6$	0.90$_8$	0.91$_3$	0.91$_4$
0.5	0.88$_9$	0.89$_8$	0.90$_3$	0.90$_9$	0.90$_8$	0.92$_3$	0.91$_8$
0.6	0.89$_9$	0.90$_8$	0.90$_9$	0.90$_3$	0.92$_3$	0.92$_6$	0.92$_1$
0.7	0.90$_8$	0.90$_8$	0.90$_9$	0.92$_2$	0.92$_4$	0.93$_3$	0.93$_1$
0.8	0.90$_4$	0.91$_2$	0.92$_0$	0.92$_2$	0.92$_4$	0.92$_2$	0.93$_3$
0.9	0.91$_2$	0.90$_2$	0.91$_1$	0.91$_6$	0.91$_8$	0.92$_2$	0.91$_9$
1.0	0.88$_7$	0.89$_7$	0.89$_2$	0.89$_7$	0.90$_3$	0.91$_9$	0.91$_1$

x cm	cos D_7	cos D_8	cos D_9	cos D_{10}	cos D_{11}	cos D_{12}	cos D_{13}
0	0.88$_3$	0.88$_3$	0.89$_1$	0.89$_3$	0.90$_3$	0.90$_5$	0.91$_0$
0.1	0.88$_8$	0.90$_2$	0.90$_5$	0.91$_4$	0.91$_3$	0.92$_2$	0.91$_8$
0.2	0.90$_1$	0.90$_9$	0.91$_9$	0.91$_4$	0.91$_8$	0.93$_0$	0.92$_7$
0.3	0.91$_2$	0.92$_2$	0.92$_3$	0.92$_8$	0.92$_3$	0.93$_0$	0.93$_5$
0.4	0.92$_3$	0.93$_3$	0.93$_8$	0.93$_3$	0.94$_0$	0.93$_3$	0.94$_2$
0.5	0.93$_3$	0.93$_9$	0.93$_6$	0.93$_2$	0.94$_7$	0.94$_3$	0.95$_0$
0.6	0.93$_2$	0.94$_3$	0.93$_3$	0.94$_7$	0.94$_4$	0.94$_7$	0.95$_0$
0.7	0.93$_5$	0.93$_2$	0.94$_6$	0.94$_3$	0.94$_1$	0.94$_8$	0.94$_8$
0.8	0.92$_7$	0.93$_5$	0.93$_3$	0.94$_2$	0.94$_2$	0.94$_3$	0.94$_6$
0.9	0.91$_8$	0.92$_7$	0.93$_2$	0.93$_2$	0.93$_0$	0.93$_7$	0.94$_0$
1.0	0.91$_7$	0.92$_0$	0.91$_8$	0.92$_2$	0.92$_4$	0.92$_9$	0.92$_6$

Determination of C^*

The value of C^* is determined by the following experiment.

Put a thin glass plate between the sample and the brass ring, and measure the counts and compare with those without it under the same condition. Denote by T' the number of counts in the former case and by T_0, in the latter. Since the glass plate is very thin, the absorption by it may be practically constant for each individual beta-rays regardless of the declination of their tracks. Hence T' is given by the following equality:

$$T'=e^{-\frac{\tau C^*}{[\cos D]}}T_0, \tag{17}$$

where τ denotes the thickness of the glass plate in gram per square centimeter, and $[\cos D]$, the mean value of $\cos D$. A preliminary experiment with the chemical pure K_2SO_4, for example, gave C^* to be $9.1\,cm^2gr^{-1}$ for the beta-ray of K^{40}.

Numerical calculation of $\Sigma G_{(n,\,n+1)}$

The numerical value of μ^* being calculated from C^* and ρ^*, the numerical value of $G_{(n,\,n+1)}$ can be calculated as given below.

At first, $\cos\beta_n$ is calculated by equalities (3–1), (3–2), (3–3) and (4), and $\cos D_n$, by (7). Cos D_n's are given in Table 1 for $X=1.0$ cm., $H=0.8$ cm. and $\Delta z=0.05$ cm.. From these $\cos D_{(n,\,n+1)}$'s are calculated after equality (16).

Then $L_{(n,\,n+1)}$'s are calculated by equality (11), in which we can disregard $\frac{\cos D_{(n,\,n+1)}}{\mu^*}$ beyond its second power allowing the error less than one per cent, and as $F'(z)$ is a correction term of the second order, $F'(0)$ will reduce to $-\frac{F_{n-1}(0)-F_{n+1}(0)}{2\Delta z}$.

The numerical integration of (14) can be perfformed applying the Simpson's rule. Since $G_{(n,\,n+1)}$ thus obtained decreases exponentially

as n increases, their summation makes approximately a convergent power series, and we need calculate up to the term, the remainder of which is less than one per cent. The larger μ^* is, the smaller is the number of the terms to be calculated.

If the thickness of the sample is less than just enough for the approximate calculation of the series, the number of counts becomes so sensitive to the thickness of the sample that the quantitative measurement becomes rather difficult. Therefore, it is desirable to measure the counts using the sample thick enough for saturation.

Some results of the numerical calculation of $\Sigma G_{(n,n+1)}$ are shown in Table 2. ρ^*'s in Table 2 were obtained from $C^*=\frac{\mu^*}{\rho^*}$ using C^* for K^{40}. As is evident from the Table, difference of ρ^*'s makes no appreciable difference of $\Sigma G_{(n,n+1)}$ derived from them. The values intermediate between two and not given in the Table may be calculated as proportional to the two relevant ρ's.

Table 2. The calculated value of $\Sigma G_{(n,n+1)}$

μ^*	5	10	15	20	25
ρ^* when $C^*=9.1\,\mathrm{cm^2\,gr^{-1}}$	0.55	1.11	1.66	2.22	2.75
$\Sigma G_{(n,n+1)}$ for $H=0.8$; x, 0~1.0	0.115	0.119	0.123	0.125	
$\Sigma G_{(n,n+1)}$ for $H=1.0$; x, 0~1.0		0.096	0.099	0.102	0.103
$\Sigma G_{(n,n+1)}$ for $H=1.0$; x, 0.4~1.0		0.078	0.080	0.082	0.083
Thickness of the sample just enough for saturation (cm)	0.6	0.4	0.3	0.25	0.25

In order to ascertain the validity of the calculation of $\Sigma G_{(n,n+1)}$, we can apply the following check.

Since in equality (15), the term $\Sigma G_{(n,n+1)}$ exclusively concerns the distance H, the ratio between two T's at two H's is equal to the ratio between the two corresponding $\Sigma G_{(n,n+1)}$, whatever the values the other terms may take, namely

$$T_{H_2} : T_{H_1} = \Sigma G_{(n,n+1)H_2} : \Sigma G_{(n,n+1)H_1} \qquad (18)$$

For example, measuring the chemical pure K_2SO_4 at H=0.8 cm. and 1.0 cm., we obtained the ratio $T_{H_2} : T_{H_1}$ as 0.82, and the corresponding calculated ratio $\Sigma G_{(n,n+1)H_2} : \Sigma G_{(n,n+1)H_1}$ was 0.81. Taking the accuracy of the measurement into account, the result is satisfactory.

Determination of W

W is characteristic of each Geiger-Mueller counter. The preceding calculations have taken care of all the terms of equality (15) excepting W, which can be derived by comparing $T_{\text{calc}}(W=1)$ and T_{obs}, the experiment being carried out under the same conditions as specified in calculation, thus

$$W = \frac{T_{\text{obs}}}{T_{\text{calc}}(W=1)} . \tag{19}$$

For example, using pure K_2SO_4, we found W to be 0.86, and using potash feldspar of known chemical composition, 0.84 for the same counter.

Assuming that W solely concerns the absorption by the window, W has been calculated to be 0.90 for the same counter. Since the effect due to the absorption by air is considered to be no more than 0.01, it is obvious that there are some other factors influencing W.

Determination of p and N

Equality (15) can be used also for obtaining p or N from T experimentally determined, if either one or the other is unknown. That is, either the content of a beta-active isotope in the sample or the number of beta-rays emitted by the beta-active isotope per gram per second can be determined by measurement of the number of counts of beta-rays from the sample by means of a mica-window Geiger-Mueller counter, always with the error being assumed less than one per cent.

Discussion

Notwithstanding the several factors that might affect it, the absorption of beta-ray is usually expressed by an exponential function up to a certain thickness of the absorber. In calculating absorption coefficient the author has taken into consideration the number, instead of intensity, of beta-rays, based upon the assumption that the number of beta-rays passing through an absorber decreases exponentially. That this assumption is at least a good approximation has been confirmed by experiments so far.

On the other hand, C^*, a number corresponding to the mass absorption coefficient, in our calculation has been assumed to be a constant for a definite beta-active isotope. Although this assumption may be a good approximation when the error up to ten per cent is allowed, it is doubtful whether it is justified when more accuracy is needed. Details are to be decided experimentally.

The fluctuation of W above mentioned might be caused by C^* which may not be a constant as assumed. If so, W may differ from sample to sample, but may not fluctuate so much for a definite sample. To ascertain this experiment should be repeated on many different samples.

Summary

The number of counts per minute of beta-rays detected by a mica-window Geiger-Mueller counter has been given by the following formula:

$$T=60\frac{\pi pNW}{C^*}\sum_n G_{(n,n+1)},$$

where $\Sigma G_{(n,n+1)}$ is calculated from X, the radius of the cylinder cathode of the counter, H, the distance between the end point of the central wire of the counter and the surface of the sample, and μ^*, the absorption coefficient of the number of beta-ray passing

through the sample; the values of C^* and W can be determined by experiment.

If either p, the content of a beta-active isotope in the sample, or N, the number of beta-rays emitted by the beta-active isotope per gram per second, is unknown, it can be determined by measuring T by means of a mica-window beta counter.

Some preliminary experiments have confirmed the validity of calculation. Yet, in order to ascertain the accuracy further experiments are needed. A full description of apparatus and procedure will be described later.

Acknowledgement

The writer wishes to express his gratitude to Professor T. Ito, Institute of Mineralogy, University of Tokyo, for critically reading the manuscript, and to Dr. F. Yamasaki, Scientific Research Institute, and Professor Y. Kawada, Institute of Mathematics, College of General Education, University of Tokyo, who gave the writer many valuable advices. Thanks are also due to Dr. S. Fukagawa and the staff of Japan Radio Co. Ltd., who kindly offered me the apparatus for experiment. The writer is indebted to Messrs. Y. Takano and Y. Sato for their assistance during the experiment.

This investigation was aided by a grant from the Scientific Research Fund of the Department of the Education.

References

1) Berne, E.: Rev. Sc. Instr., 22, 509 (1951).
2) Cook, G. B., J. F. Duncan and M. A. Hewitt: Nucleonics, 8, 24 (1951).

Manuscript received July 30, 1954.

MINERALOGICAL JOURNAL, VOL. 1, NO. 3, PP. 185-187, OCT., 1954

SHORT COMMUNICATIONS

PARALLEL INTERGROWTH OF PYROXENE AND AMPHIBOLE IN PLUTONIC ROCKS*

TEIROKU SUENO

Tokyo Medical and Dental University

Introduction

Pyroxene and amphibole, when they are coexistent with each other in plutonic rocks, usually form a characteristic intergrowth. It resembles dapple under the microscope (Fig. 1, Plate I), with irregular patches of amphibole, all with the same orientation, dispersed in a single crystal of pyroxene. Sometimes the relation between them is reversed.

The writer has examined the crystallographic relationship of the typical intergrowth of this type.

Observation under the microscope

To determine the crystallographic orientation of thin sections, it is usual to use a universal stage. However, the writer has achieved the same object using the diagrams** for determining the orientation of thin sections. Figs. 2 and 3 (Plate II) show ones for amphibole and poroxene respectively. They give in stereographic projection the variation of the angles between traces of (110), ($1\bar{1}0$), (100) and

* Dedicated to Dr. S. Tsuboi, Emeritus Professor of University of Tokyo, on the occasion of his sixtieth birthday.

A preliminary report was read at the Annual Meeting of the Geological Society of Tokyo held in April, 1931.

** The description of the diagrams is to be printed in the Journal of the Mineralogical Society of Japan, Vol. 2, No. 2 (in Japanese).

(010) in contours of 5° or 10° apart.

(110) (and $(1\bar{1}0)$) being a perfect cleavage its traces can be clearly observed in dark field. The traces of (100) can be determined by observing the trace of the composition-plane of twin under crossed nicols, while those of (010) can be determined by noting the emergence of the optical plane.

Using this method the writer observed many thin sections of amphibole and pyroxene from the basic plutonic rocks from Nishidohira[2)3)], and found that they are all intergrown in the approximately parallel position, each of the crystallographic axes of the one being parallel, or nearly parallel, to the relevant axis of the other. The parallelism is ascertained within the accuracy of 5°. It is to be noticed that, when host pyroxene is twinned, amphibole inclosed in patches is also twinned and the twinned halves are united by strictly the same composition-plane in both of them (Fig. 1A, Plate I).

X-ray experiment

A number of cleavage pieces of pyroxene intimately intergrown with amphibole were *X*-rayed taking rotation photographs about the *c*-axis (Fig. 4, Plate I). They, too, demonstrate that the two crystals are intergrown in parallel.

Discussion

It is known that amphibole overgrown on pyroxene is also arranged approximately in parallel positions[1)4)]. The intergrowth in patches described above indicates that under plutonic condition, transformation of pyroxene into its reaction partner, amphibole, might start not only along the rim in contact with magmatic liquid but also at arbitrary points of the pyroxene crystal. Contrary to pyroxene and amphibole, olivine and rhombic pyroxene, another reaction pair in plutonic rocks, usually form a reaction rim.

In conclusion the writer wishes to express his sincere thanks to Professor Seitaro Tsuboi for his guidance during the course of this investigation.

References

1) Inuzuka, H.: Beitr. Miner. Japan, N. F. 1, 148 (1935).
2) Sueno, T.: Jour. Geol. Soc. Tokyo, 38, 275 (1931).
3) Watanabe, M.: Sc. Rep. Tohoku Imp. Univ., 3rd Ser., 1, 33 (1923).
4) Williams, G. H.: Am. Jour. Sc., 139, 358 (1890).

(A) ×120

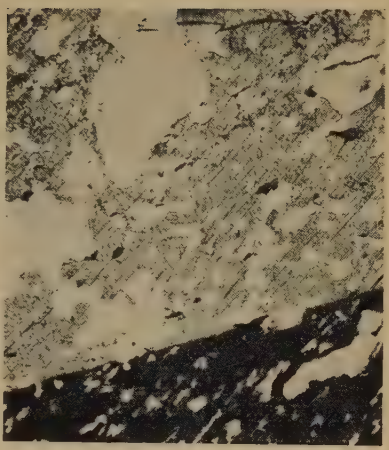

(B) ×120

Fig. 1. Pyroxene intergrown with amphibole.

(A) Dark and grey parts: amphibole twinned. Light part: pyroxene.
(B) Diagonal to (A). Dark and grey parts: pyroxene twinned. Light part: amphibole.

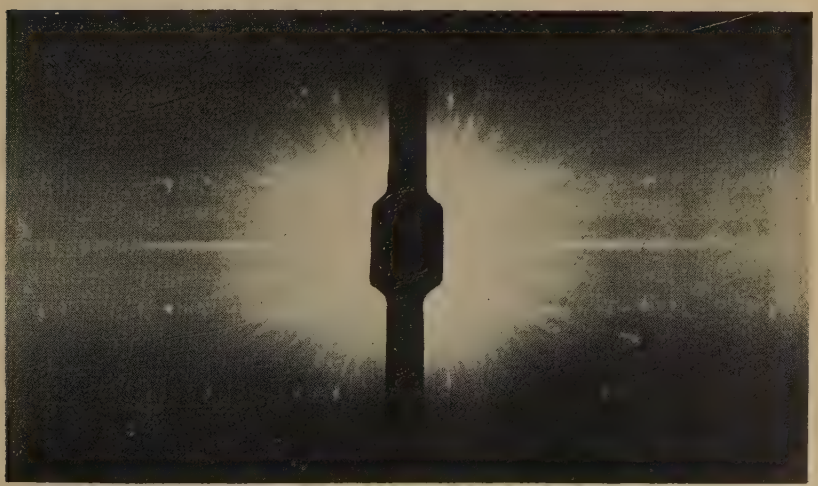

Fig. 4. X-ray rotation photograph of intergrown pyroxene and amphibole. Rotation axis c. Cu k_{α}.

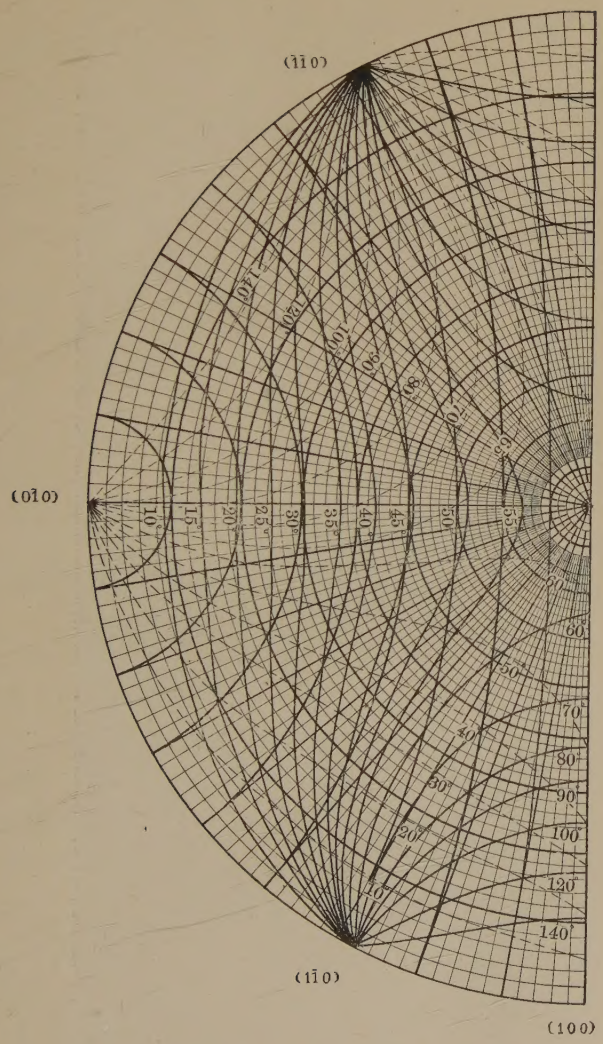

Fig. 2. Diagram for determining orientation of thin sectoin of hornblende.

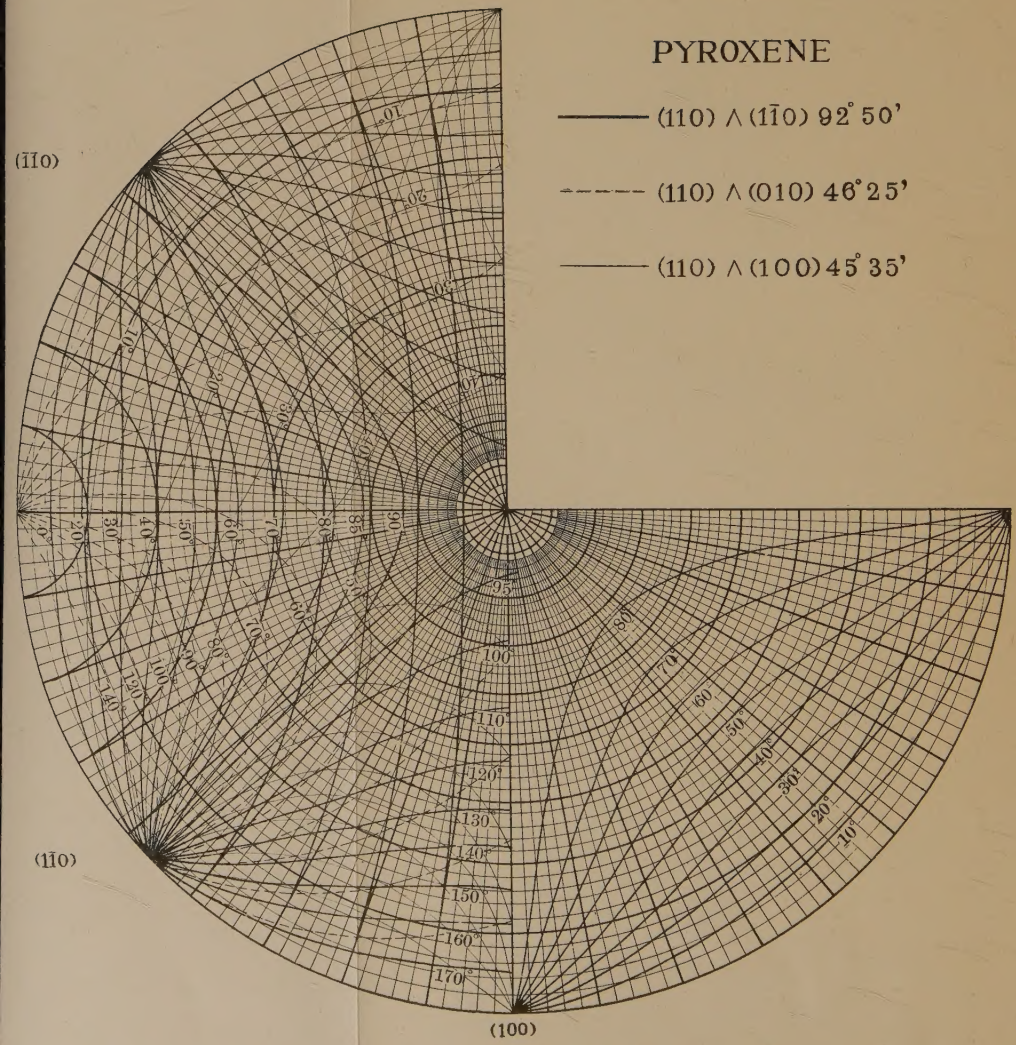

Fig. 3. Diagram for determining orientation of thin section of pyroxene.

Contents of "KOBUTSUGAKU ZASSHI,"

Journal of the Mineralogical Society of Japan

in Japanese

VOL. 1, No. 6 (May, 1954)

Original Articles

On the Digenite from Ōjamine Mine, Yamagata Prefecture ..... T. Takeuchi and M. Nambu...373

Chemical Analysis of Calcite Group and the Crystal-chemical Consideration about it .....Z. Harada and S. Matsuda...380

Colour of Zincblende from the Hosokura Mine, Miyagi Prefecture ..... K. Togari...391

Studies on Magnetite from Kayaki-mura, Nishisonogi-gun, Nagasaki prefecture..... G. Shibuya...403

On the Apophyllite from the Shin-yama, Kamaishi Mine..... H. Minato, N. Wada and S. Tsurushima...414

Studies on the Chemical Analysis of Several Ores with Regard to their Mineral Composition. (Part 1) General Introduction.....T. Imai...422

(Part 2) Mangan Ore...T. Imai and Y. Kaneko...424

Short Communications

On Twin Crystals of Alabandite from the Inakuraisi Mine, Siribesi Province, Hokkaido .....Z. Harada...433

Communications on Minerals of Japan (Part 4).....Mumeikai Group...435

8. Rutile from Kuwanokawa, Kōchi Prefecture..... K. Sasakura and K. Sakurai

9. Fibroferrite from Yamané, Tottori Prefecture ..... K. Sakurai and T. Ashizawa

Proceedings 441

Index to volume 1.....443

Printed by "HERALD" Printing Co., Ltd.

Contents of "KOBUTSUGAKU ZASSHI,"

Journal of the Mineralogical Society of Japan

in Japanese

VOL. 2, No. 1 (September, 1954)

Addresses

Hokutolites from the Hot Spring Tamagawa ..... E. Minami... 1

Original Articles

Geiger Counter Measurement of Radiation of Monazite from Ishikawa, Fukushima Prefecture ..... K. Omori...25

Piedmontite from Tone, Nagasaki Prefecture ..... F. Hirowatari...33

Pyromorphite from the Nabeto Mine, Ishikawa Prefecture ..... S. Sugiura...39

Short Communications

Occurrence of Skarn Minerals at Hashikake-zawa, Sekkai-zawa and Deai in the Chichibu Mine ..... N. Katayama, Y. Takano, I. Kato, T. Kato and S. Nakagawa...46

Communications on Minerals of Japan (Part 5) ..... Mumeikai Group...53

10. Fluorite from Igashima Mine, Niigata Prefecture ..... S. Takasu
11. Pectolite from Awashima, Niigata Prefecture ..... K. Sakurai
12. Cervantite from Tateishi Town, Oita Prefecture ..... K. Sakurai

Reviews

Foundation of Thermodynamics in the Scope of Mineralogy ..... T. Sudo...61

Proceedings 73